

Holographic CFT phase transitions for 4-D Dyonic AdS black holes

Abhishek Baruah, Prabwal Phukon

Department Of Physics,

Dibrugarh University, Dibrugarh, 786004, Assam, India

Theoretical Physics Division, Centre for Atmospheric Studies, Dibrugarh University, Dibrugarh, 786004, Assam, India

E-mail: rs_abhishekbaruah@dibru.ac.in, prabwal@dibru.ac.in

ABSTRACT: From the AdS/CFT correspondence framework, we inspect the holographic conjugate of the of 4 – D extended charged dyonic Anti-de-Sitter black hole thermodynamics. With the alterations in Λ as cosmological constant and G_N as the Newton’s constant, the AdS black holes gravitational thermodynamics can be extended. This relates to incorporating the C as CFT central charge and μ as its chemical potential to the standard pairs of (T, S) that is temperature vs. entropy, $(\tilde{\Phi}, \tilde{Q})$ as electric potential vs. charge, and (p, \mathcal{V}) as field theory pressure vs. volume as a nascent pair in the dual CFT for conjugate thermodynamic variables. Here we taken to explore the dyonic system. So the traditional pairs for potential and charges become $(\tilde{\Phi}_e, \tilde{Q}_e)$ as electric potential and charge and $(\tilde{\Phi}_m, \tilde{Q}_m)$ as magnetic potential and charge. In the exploration of all ensembles, we found that only some show interesting phase behaviour. Namely, $(\tilde{\Phi}_e, \tilde{Q}_m \mathcal{V}, C)$, $(\tilde{\Phi}_e, \tilde{Q}_m \mathcal{V}, \mu)$, $(\tilde{Q}_e, \tilde{\Phi}_m \mathcal{V}, C)$, $(\tilde{Q}_e, \tilde{\Phi}_m \mathcal{V}, \mu)$, $(\tilde{\Phi}_e, \tilde{\Phi}_m \mathcal{V}, C)$, $(\tilde{Q}_e, \tilde{Q}_m \mathcal{V}, C)$, $(\tilde{Q}_e, \tilde{Q}_m \mathcal{V}, \mu)$. For ensembles $(\tilde{\Phi}_e, \tilde{Q}_m \mathcal{V}, C)$, $(\tilde{\Phi}_m, \tilde{Q}_e \mathcal{V}, C)$ and $(\tilde{Q}_e, \tilde{Q}_m \mathcal{V}, C)$ we notice a change of phase of order one and two. For the ensemble $(\tilde{\Phi}_e, \tilde{\Phi}_m \mathcal{V}, C)$ we observe a confined/deconfined phase transition. At a temperature that relies on μ , we observe a change of phase of order one between the phases of high- and low-entropy in the fixed $(\tilde{\Phi}_e, \tilde{Q}_m \mathcal{V}, \mu)$, $(\tilde{\Phi}_m, \tilde{Q}_e \mathcal{V}, \mu)$, $(\tilde{Q}_e, \tilde{Q}_m \mathcal{V}, \mu)$. In our exploration of the parametric graphs, the fixed p ensembles namely $(\tilde{\Phi}_e, \tilde{Q}_m, p, C)$, $(\tilde{\Phi}_e, \tilde{Q}_m, p, \mu)$, $(\tilde{\Phi}_m, \tilde{Q}_e, p, C)$, $(\tilde{\Phi}_m, \tilde{Q}_e, p, \mu)$, $(\tilde{\Phi}_m, \tilde{\Phi}_e, p, C)$, $(\tilde{\Phi}_m, \tilde{\Phi}_e, p, \mu)$, $(\tilde{Q}_m, \tilde{Q}_e, p, C)$, $(\tilde{Q}_m, \tilde{Q}_e, p, \mu)$ exhibit no critical behavior, or $p - \mathcal{V}$ criticality, the conjugate state of the CFT linked to a classical dual charged Anti-de-Sitter black holes cannot be seen as Van der Waals fluid.

Contents

1	A brief introduction	1
2	Holographic thermodynamics of dyonic Anti-de-Sitter black holes	4
2.1	Extended phase space thermodynamics of Dyonic Anti-de-Sitter black holes	4
2.1.1	For Φ_e and Q_m	6
2.1.2	For Φ_m and Q_e	6
2.1.3	For Φ_e and Φ_m	7
2.1.4	For Q_e and Q_m	7
2.2	The thermodynamics of Conformal Field Theory (CFT) with a central charge C and the chemical potential μ	7
2.3	Energy (E), temperature (T) and chemical potential (μ) for $(\tilde{\Phi}_e, \tilde{Q}_m)$	10
2.4	Energy (E), Temperature (T) and chemical potential (μ) for $(\tilde{\Phi}_m, \tilde{Q}_e)$	10
2.5	Energy (E), Temperature (T) and chemical potential (μ) for $(\tilde{\Phi}_e, \tilde{\Phi}_m)$	10
2.6	Energy (E), Temperature (T) and chemical potential (μ) for $(\tilde{Q}_e, \tilde{Q}_m)$	11
3	Different types of ensembles in the CFT thermodynamics	11
3.1	For the fixed $(\tilde{Q}_m, \tilde{\Phi}_e, \mathcal{V}, C)$ ensemble	12
3.2	For the fixed $(\tilde{Q}_m, \tilde{\Phi}_e, \mathcal{V}, \mu)$ ensemble	15
3.3	For the fixed $(\tilde{Q}_e, \tilde{\Phi}_m, \mathcal{V}, C)$ ensemble	19
3.4	For the fixed $(\tilde{Q}_e, \tilde{\Phi}_m, \mathcal{V}, \mu)$ ensemble	22
3.5	For the fixed $(\tilde{\Phi}_e, \tilde{\Phi}_m, \mathcal{V}, C)$ ensemble	26
3.6	For the fixed $(\tilde{\Phi}_e, \tilde{\Phi}_m, \mathcal{V}, \mu)$ ensemble	28
3.7	For the fixed $(\tilde{Q}_e, \tilde{Q}_m, \mathcal{V}, C)$ ensemble	28
3.8	For the fixed $(\tilde{Q}_e, \tilde{Q}_m, \mathcal{V}, \mu)$ ensemble	31
4	The rest of the ensembles	34
5	Discussions	37

1 A brief introduction

In the cosmic fabric of spacetime, where light bends and time warps, black holes are the cosmic enigmas and a source of gravitational singularity derived from general relativity. Black holes are being considered to mimic black bodies once the quantum effects are considered since they are taken as nature's ideal absorbers. For approximately half a century, thermodynamics of black holes has been the centre of extensive study. There is two main phases to thermodynamics of black hole. Bekenstein, Bardeen, [1, 2] Carter, Hawking, and others [3, 4] pioneered the first and initial stage. Conventional black hole thermodynamics

(TBHT) is the formalism or concept developed at this phase. Black hole mass is regarded as the internal energy, and black hole temperature is determined by its angular momentum, mass, charge, in addition to other physical setup-related parameters. Contrary to a fluid like system, where entropy corresponds to volume, conjugate thermodynamic entropy in Einstein's gravity is directly proportional to the A , that is the horizon area.

We set $\hbar = c = k_B = 1$, we consider the Hawking temperature T and Bekenstein-Hawking entropy S of dyonic AdS black holes is given as [5–9]-

$$T = \frac{\kappa}{2\pi}, \quad S = \frac{A}{4G_N} \quad (1.1)$$

where in (1.1), the surface gravity is κ and G_N is the Newton constant.

One class of black holes that created immense expansion in the study of thermodynamics of black holes is the asymptotically AdS (Anti-de-Sitter) black holes. Based on their ensembles and types (hairy, rotating, charged, uncharged, both charged and rotating) they are characterized by rich phase structures. Currently, there are other ways of studying the rich phase structures [10–12], using certain tools like the thermodynamic geometry [13–20] and the thermodynamic topology. [24–37]

Asymptotically, the AdS (Anti-de-Sitter) black holes also known as holographic theory, which are analogous to thermal boundary states in the dual (CFT) conformal field theory. [38], greatly enhances the thermodynamics of black holes. The breakthrough of the Hawking-Page phase transition [39] for the Anti-de-Sitter (AdS) black holes is another significant advance in this direction. This is a alteration of phase from a state of black hole to a completely state of thermal gas, distinguished by diminishing Gibbs free energy.

The second phase is the (EPST) Extended Phase Space Thermodynamics[40–48]. The formalism was introduced by scientists namely Kastor, Traschen and Ray [49] and then it was further developed by more researchers. The main advancement at this stage is the addition of a new set of variables, like the negative cosmological constant Λ (which is proportional to thermodynamic pressure P), and its complimentary variable, the thermodynamic volume V . Interpreting mass parameter as the enthalpy is the price paid for this modification in this formalism. Asymptotically, the charged AdS (Anti-de-Sitter) black holes can achieve steady state (thermal equilibrium) with their Hawking radiation and is obtained to display a variety of intriguing behaviours in the phase, such as transition to radiation which is a first-order that corresponds to the confinement or de confinement of the dual quark-gluon plasma [50] and many more. [51–59]. Anti -de-Sitter black holes can also be considered as heat engines thanks to the presence of the (P, V) variables [60, 61]. All these phenomena listed above have been found out via the concept of the thermodynamics of the extended phase space, where pressure P is identified with Λ i.e the cosmological constant.

$$P = -\frac{\Lambda}{8\pi G_N}, \quad \Lambda = -\frac{(d-1)(d-2)}{2L^2} \quad (1.2)$$

Most recently, Visser [62] added a new pair of complimentary thermodynamic variables to the research of Extended Phase Space Thermodynamics by taking the chemical potential

μ and the central charge C . This extension of the fundamental law of the thermodynamics of black holes, the investigation of the related criticality on central charge C has recently come into existence [63, 64].

In the backdrop of the ADS/CFT correspondence, in the paper [65] they have examined the holographic counterpart of the extended thermodynamics of spherically symmetric, charged Anti-de-Sitter black holes by allowing variations of the Newton's constant G_N and the cosmological constant Λ . Also the chemical potential μ and central charge C are included in the dual CFT. In paper [66, 67], they have done the same analysis but with a rotating AdS black hole. AdS black holes exhibit enriched phase behavior because of the inclusion of a cosmological constant Λ that is negative. There are some novel phase transitions are acquired by addressing the cosmological constant Λ as an extra variable for the black holes. Since Newton's constant G_N can be considered as a coupling constant that can alter in the gravitational theories space and, fluctuates along the renormalization group flow if quantum revisions are taken into account, it has recently been listed to the extended thermodynamic phase space (EPST) as a parameter that can be altered [68–71]. Within the idea of AdS/CFT correspondence based on Visser's idea, a nascent formalism was given by Ghao and Zhao popularised as the 'restricted phase space (RPS) thermodynamics' [72]. This formalism has the freedom from pressure P and volume V and interprets the mass as the internal energy. Several literature review have been done using this concept or formalism. [73–77]

The basic thermodynamical characteristics of charged (electrically) black holes at arbitrary diameters are widely understood. However, due to the electromagnetic duality, a black hole can be created in the four space-time dimensions that can transport electric and magnetic charges. This sort of black holes are categorised as a dyonic black hole. In the literature [78] they explored a dual charged black hole in asymptotically Anti-de-Sitter spacetime in the quest to gain knowledge of the thermodynamic features of its complimentary CFT boundary.

A dyonic (dual-charge) black hole consists of the U(1) gauge and the graviton (metric) fields. This metric fulfils the Anti-de-Sitter boundary, and then the 2 alternative boundary conditions for the gauge field, the first is a mode that can be normalized and is associated with the vacuum expectation value (VEV) of the corresponding dual operator, and the second is a mode that cannot be normalized corresponding to the use of an gauge field which is external which alters the theory at the boundary. The existence of a magnetic monopole adds complexity to the phase diagram of the Anti-de-Sitter spacetime black holes. Deformed dimensional field theories have recently received considerable attention in the presence of a holographic interpretation of certain phenomena such as superconductivity/superfluidity [79], the Hall effect [80], magnetohydrodynamics [81–83], the Nernst effect [84] and many more [85–90].

Black hole thermodynamics is highly influenced by the choice of ensemble. As we have seen in the case of CFT thermodynamics of charged AdS black holes, out of the eight possible ensembles in only three ensembles phase transitions are observed. To understand the

intricate relationship between the nature of ensemble and phase transitions in holographic thermodynamics, it is pertinent that one explores black holes with more and diverse set of thermodynamic ensembles. The dual CFT corresponding to 4-D charged dyonic AdS black hole is enriched with 16 different ensembles. The presence of ensembles in addition to the ones available in the case of dual CFT of charged AdS black holes makes it a perfect choice to investigate the dependence of CFT phase structure on the nature of ensembles. The introduction of both the electric and magnetic charges together may introduce some new interactions which might not be present in purely electrical-charged systems. These combinations can change the thermodynamic potentials and their corresponding functions which leads to a combination of fixed for varying charges and potential both electric and magnetic. This can be referred to as mixed ensembles. A dual charged black hole is capable to show richer phase structure such as criticality depending on both the charges.

In this study, we further explore the holographic counterpart of the thermodynamics in the extended phase space of the dyonic Anti-de-Sitter black holes. There are a total of 16 potential thermodynamic (grand) canonical and mixed ensembles in the CFT for the four conjugate quantities $(\tilde{\Phi}_e, \tilde{Q}_e)$, $(\tilde{\Phi}_m, \tilde{Q}_m)$, (p, \mathcal{V}) and (μ, C) . Section 3, we discover that seven of the ensembles— the ensembles at fixed $(\tilde{\Phi}_e, \tilde{Q}_m, \mathcal{V}, C)$, $(\tilde{\Phi}_e, \tilde{Q}_m, \mathcal{V}, \mu)$, $(\tilde{\Phi}_m, \tilde{Q}_e, \mathcal{V}, C)$, $(\tilde{\Phi}_m, \tilde{Q}_e, \mathcal{V}, \mu)$, $(\tilde{\Phi}_e, \tilde{\Phi}_m, \mathcal{V}, C)$, $(\tilde{Q}_e, \tilde{Q}_m, \mathcal{V}, C)$, $(\tilde{Q}_e, \tilde{Q}_m, \mathcal{V}, \mu)$ ensembles exhibits fascinating phase behavior or critical events. We evaluate the pertinent phase diagrams and graph the corresponding free energy in these ensembles with respect to temperature. In section 4, we plot the remaining free energy plots for the p containing ensembles. In section 5 we look into conclusions, discussions, and further works.

2 Holographic thermodynamics of dyonic Anti-de-Sitter black holes

The bulk thermodynamics of AdS black holes and the complimentary CFT are related by the AdS/CFT correspondence. For the extended thermodynamics of dual charge Anti-de-Sitter black holes the holographic dictionary is described and reviewed in this section. All charts are made for $d \rightarrow 3$, or the AdS_4/CFT_3 relationship because it gets too complicated to generalize in d -dimension.

2.1 Extended phase space thermodynamics of Dyonic Anti-de-Sitter black holes

The Reissner-Nordström action in the existence of a negative cosmological constant Λ are given as-

$$I = \frac{1}{16\pi G_4} \int d^4x \sqrt{g} (-R + F^2 - \frac{6}{L^2}) \quad (2.1)$$

The equations of motion are-

$$R_{\mu\nu} - \frac{1}{2}g_{\mu\nu}R - \frac{3}{L^2}g_{\mu\nu} = 2(F_{\mu\lambda}F_{\nu}^{\lambda} - \frac{1}{4}g_{\mu\nu}F_{\alpha\beta}F^{\alpha\beta}) \quad (2.2a)$$

$$\nabla_{\mu}F^{\mu\nu} = 0 \quad (2.2b)$$

These equations have a static, spherically symmetric solution provided by

$$A = \left(-\frac{q_e}{r} + \frac{q_m}{r_+} \right) dt + (q_m \cos \theta) d\phi \quad (2.3)$$

and

$$ds^2 = -f(r)dt^2 + \frac{1}{f(r)}dr^2 + r^2 d\theta^2 + r^2 \sin^2 \theta d\phi^2 \quad (2.4)$$

where the electromagnetic four-potential is A and

$$f(r_+) = \left(1 + \frac{r_+^2}{L^2} - \frac{m}{r_+} + \frac{q_e^2 + q_m^2}{r_+^2} \right) \quad (2.5)$$

where in (2.5), q_e , is the electric charge, q_m is the magnetic charge, and m is and ADM mass parameter of the blackhole.

The ADM mass is connected to the mass parameter of the blackhole as

$$M = \frac{(d-1)\Omega_{d-1}}{16\pi G_N} m \quad (2.6)$$

Putting $d=3$ as stated before we get the ADM mass as:-

$$M = \frac{2\Omega_2}{16\pi G_N} m \quad (2.7)$$

Putting solid angle, $\Omega_2=4\pi$ on (2.7) we get the mass parameter connected to the ADM mass as-

$$M = \frac{m}{2G_N} \quad (2.8)$$

and the Berkenstein-Hawking entropy is given as

$$S = \frac{\Omega_{d-1} r_+^{d-1}}{4G_N} \quad (2.9)$$

Further, the electric charge parameter q_e can be connected to the Q_e electric charge via-

$$Q_e = \frac{(d-1)\Omega_{d-1}}{8\pi G_N} \alpha q_e \quad \text{and} \quad \alpha = \sqrt{\frac{2(d-2)}{d-1}} \quad (2.10)$$

for the entire calculation we are using $d = 3$ and for that we apply $\Omega_2 = 4\pi$ and $\alpha = 1$. Therefore we get from (2.10),

$$Q_e = \frac{q_e}{G_N} \quad \text{and similarly} \quad Q_m = \frac{q_m}{G_N} \quad (2.11)$$

Additionally, we operate in an ensemble where A_t has a constant asymptotic value. Hence we get:-

$$\Phi_e = \frac{q_e}{r_+}, \quad \text{and} \quad \Phi_m = \frac{q_m}{r_+} \quad (2.12)$$

With this decision, Φ_e and Φ_m stand for any hypothetical distinction between infinity and the outside horizon. The generalized Smarr formula relates the black hole parameters to one another as,

$$M = \frac{d-1}{d-2} \frac{\kappa A}{8\pi G_N} + \Phi_e Q_e + \Phi_m Q_m - \frac{1}{d-2} \frac{\Theta \Lambda}{4\pi G_N} \quad (2.13)$$

Putting $f(r_+) = 0$ in (2.5) we can calculate the mass as,

$$\left(1 + \frac{r_+^2}{L^2} - \frac{m}{r_+} + \frac{q_e^2 + q_m^2}{r_+^2}\right) = 0$$

$$m = \frac{\frac{r_+^4}{L^2} + q_e^2 + q_m^2 + r_+^2}{r_+} \quad (2.14)$$

In this study, we first have 4 different kinds of consideration which will be modified later. We take:-

1. Φ_e and Q_m fixed
2. Φ_m and Q_e fixed
3. Φ_e and Φ_m fixed
4. Q_e and Q_m fixed

2.1.1 For Φ_e and Q_m

We will work on an ensemble where the quantities Φ_e and Q_m are fixed. Hence the Φ_e electric potential is described as-

$$\Phi_e = \frac{q_e}{r_+} \quad (2.15)$$

Hawking temperature of the dyonic Anti-de-Sitter black hole is

$$T_1 = \frac{\kappa}{2\pi} = \frac{f'(r_+)}{4\pi}$$

$$= \frac{\frac{2r_+}{L^2} + \frac{m}{r_+^2} - \frac{2(q_e^2 + q_m^2)}{r_+^3}}{4\pi} = -\frac{-\frac{3r_+^4}{L^2} + q_e^2 + q_m^2 - r_+^2}{4\pi r_+^3} \quad (\text{Putting } m \text{ from (2.14)}) \quad (2.16)$$

$$T_1 = \frac{1}{4\pi r_+} \left(1 + \frac{3r_+^2}{L^2} - \Phi_e^2 - \frac{q_m^2}{r_+^2}\right)$$

2.1.2 For Φ_m and Q_e

For this, take the quantities Φ_m and Q_e as fixed. Here the magnetic potential is defined as:-

$$\Phi_m = \frac{q_m}{r_+} \quad (2.17)$$

Hawking temperature of the dyonic Anti-de-Sitter black hole is

$$T_2 = \frac{\kappa}{2\pi} = \frac{f'(r_+)}{4\pi}$$

$$= \frac{\frac{2r_+}{L^2} + \frac{m}{r_+^2} - \frac{2(q_e^2 + q_m^2)}{r_+^3}}{4\pi} = -\frac{-\frac{3r_+^4}{L^2} + q_e^2 + q_m^2 - r_+^2}{4\pi r_+^3} \quad (\text{Putting } m \text{ from (2.14)}) \quad (2.18)$$

$$T_2 = \frac{1}{4\pi r_+} \left(1 + \frac{3r_+^2}{L^2} - \Phi_m^2 - \frac{q_e^2}{r_+^2}\right)$$

2.1.3 For Φ_e and Φ_m

For this take the quantities Φ_m and Φ_e as fixed. The electric and magnetic potential are:-

$$\Phi_e = \frac{q_e}{r_+}, \quad \Phi_m = \frac{q_m}{r_+} \quad (2.19)$$

Hawking temperature for the dyonic Anti-de-Sitter black hole is:-

$$\begin{aligned} T_3 &= \frac{\kappa}{2\pi} = \frac{f'(r_+)}{4\pi} \\ &= \frac{\frac{2r_+}{L^2} + \frac{m}{r_+^2} - \frac{2(q_e^2 + q_m^2)}{r_+^3}}{4\pi} = -\frac{-\frac{3r_+^4}{L^2} + q_e^2 + q_m^2 - r_+^2}{4\pi r_+^3} \quad (\text{Putting } m \text{ from (2.14)}) \quad (2.20) \\ T_3 &= \frac{1}{4\pi r_+} \left[1 + \frac{3r_+^2}{L^2} - \Phi_e^2 - \Phi_m^2 \right] \end{aligned}$$

2.1.4 For Q_e and Q_m

For this take the quantities Q_m and Q_e as fixed quantities. Hawking's temperature of the dyonic Anti-de-Sitter black hole is:-

$$\begin{aligned} T_4 &= \frac{\kappa}{2\pi} = \frac{f'(r_+)}{4\pi} \\ &= \frac{\frac{2r_+}{L^2} + \frac{m}{r_+^2} - \frac{2(q_e^2 + q_m^2)}{r_+^3}}{4\pi} = -\frac{-\frac{3r_+^4}{L^2} + q_e^2 + q_m^2 - r_+^2}{4\pi r_+^3} \quad (\text{Putting } m \text{ from (2.14)}) \quad (2.21) \\ T_4 &= \frac{1}{4\pi r_+} \left(1 + \frac{3r_+^2}{L^2} - \frac{q_e^2}{r_+^2} - \frac{q_m^2}{r_+^2} \right) \end{aligned}$$

By relating to a scaling argument in [91, 92], first law mechanics for the charged dyonic AdS black hole can be stretched to the generalized Smarr formula. The L which is the AdS radius is being scaled with the black hole parameters as $M \sim L^{d-2}$, $A \sim L^{d-1}$, $Q \sim L^{d-2}$ and also $\Lambda \sim L^{-2}$, similarly with Newton's constant of gravitation, we get the scaling as $M, Q \sim G_N^{-1}$. First law of gravitation for the charged dyonic Anti-de-Sitter black holes stretches to incorporate alterations of the theoretical variables of the G_N gravitational constant and Λ cosmological constant are:-

$$dM = \frac{\kappa}{8\pi G_N} dA + \Phi_e dQ_e + \Phi_m dQ_m + \frac{\Theta}{8\pi G_N} d\Lambda - (M - \Phi_e Q_e - \Phi_m Q_m) \frac{dG_N}{G_N} \quad (2.22)$$

The integration of the Λ cosmological constant variation for first rule has been extensively examined in the literature, as was indicated in the introduction. The fluctuation of Newton's constant has previously been discussed in the Anti-de-Sitter black holes extended fundamental and the fundamental law of holographic entanglement entropy in [93, 94].

2.2 The thermodynamics of Conformal Field Theory (CFT) with a central charge C and the chemical potential μ

The Smarr formula (2.13) similar for Anti-de-Sitter black holes was demonstrated in [95] that has a $p\mathcal{V}$ term and lacking μC term. The dual Euler equation for charged dyonic AdS black holes is:-

$$E - TS + \tilde{\Phi}_e \tilde{Q}_e + \tilde{\Phi}_m \tilde{Q}_m + \mu C \quad (2.23)$$

Here μ is chemical potential conjugate to C which is the central charge and $\tilde{\Phi}_e$, is the CFT electric potential and \tilde{Q}_e is the CFT electric charge and $\tilde{\Phi}_m$ is the CFT magnetic potential and, \tilde{Q}_m is the CFT magnetic charge. The extended first law in (2.22), which incorporates both a $pd\mathcal{V}$ and μdC terms, was aligned with the expanded version of the CFT thermodynamics first law as-

$$dE = TdS + \tilde{\Phi}_e d\tilde{Q}_e + \tilde{\Phi}_m d\tilde{Q}_m - pd\mathcal{V} + \mu dC \quad (2.24)$$

where in (2.24), \mathcal{V} is the volume of the CFT and p is the field theory pressure.

In AdS/CFT correspondence, the bulk theory's gravitational coupling constants and the AdS radius are related to the CFT's central charge. According to this dictionary, Einstein's gravity reads as

$$C = \frac{\Omega_{d-1} L^{d-1}}{16\pi G_N} \quad (2.25)$$

The volume of space \mathcal{V} of the geometry where the CFT is placed is another CFT characteristic that is mentioned in the thermodynamic first law. The CFT is frequently placed on a sphere of L AdS radius, resulting in a volume of $\mathcal{V} = \Omega_{d-1} L^{d-1}$. We make a distinction between the CFT's volume of space \mathcal{V} and its C central charge. Consequently, we choose to make the bulk L curvature radius different from the boundary R curvature radius, and the volume is written as:-

$$\mathcal{V} = \Omega_{d-1} R^{d-1} \quad (2.26)$$

This sphere volume of radius R in the AdS bulk which is in $(d-1)$ dimensions and $\mathbf{R} \times S^{d-1}$, which relates to the 'area' in the CFT boundary which is in $(d+1)$ -dimensions. The dual field theory in AdS/CFT is located on the asymptotically AdS spacetime's conformal field theory boundary. By using the Gubser-Klebanov-Polyakov-Witten (GKPW) prescription, the AdS metric g_{AdS} is related to the CFT metric g_{CFT} when taken or utilised on the asymptotic boundary edge tending to a Weyl rescaling.[96, 97].

$$g_{\text{CFT}} = \lim_{r \rightarrow \infty} (\lambda(x) g_{\text{AdS}}) \quad (2.27)$$

where $\lambda(x)$ is a freely chosen Weyl rescale factor and $r \rightarrow \infty$ denotes spatial infinity. As $r \rightarrow \infty$, the asymptotically AdS spacetime line element approaches.

$$ds^2 = -\frac{r^2}{L^2} dt^2 + \frac{L^2}{r^2} dr^2 + r^2 d\Omega_{d-1}^2 \quad (2.28)$$

The model choice of the Weyl rescale factor $\lambda = L/r$ the line element of the edge CFT is $ds^2 = -dt^2 + L^2 d\Omega^2$. In this instance, the curvature radius of the boundary and the bulk curvature radius are the same. Instead, we'll assume that the Weyl rescale factor is $\lambda = R/r$, which places the CFT on a sphere with R as constant radius. As a result, line element of the CFT's becomes with $d=3$

$$ds^2 = -\frac{R^2}{L^2} dt^2 + R^2 d\Omega_2^2 \quad (2.29)$$

For the S entropy, E energy, T temperature, $\tilde{\Phi}_m$ magnetic potential, \tilde{Q}_m magnetic charge, $\tilde{\Phi}_e$ electric potential, \tilde{Q}_e electric charge, the holographic dictionary can be written for the choice of the above CFT metric [62]-

$$\begin{aligned} S &= \frac{A}{4G_N}, & E &= M \frac{L}{R}, & T &= \frac{\kappa}{2\pi} \frac{L}{R}, & \tilde{\Phi}_e &= \frac{\Phi_e}{L} \frac{L}{R}, \\ \tilde{Q}_e &= Q_e L, & \tilde{\Phi}_m &= \frac{\Phi_m}{L} \frac{L}{R}, & \tilde{Q}_m &= Q_m L \end{aligned} \quad (2.30)$$

Due to a factor R/L difference between the bulk and the boundary CFT time in (2.30), the rescale factor L/R occurs in the dictionaries for the temperature, energy, and electric and magnetic potential [98]. As a result, the dictionaries for energy, temperature, and potential are different from the holographic dictionaries by a factor of L/R .

The vacuum state energy vanishes in the holographic dictionary above. The counterterm subtraction approach [99, 100], is used to calculate the energy of the vacuum for a CFT. $E = (M + E_0)L/R$ is the proper dictionary for the rescaled energy that results via this approach, where the energy of the vacuum $E_0 \sim C$ corresponds to the C central charge. Since the Casimir energy has little bearing on (holographic) thermodynamics, hence disregarded.

The generalized Smarr formula (2.13) replaces Θ in the first law extension (2.22) and plug in $d\Lambda/\Lambda = -2dL/L$, which is vital in the matching of the bulk and edge/ boundary first laws [62]. Then we can write the extended first law:-

$$\begin{aligned} d\left(M \frac{L}{R}\right) &= \frac{\kappa}{2\pi} \frac{L}{R} d\left(\frac{A}{4G_N}\right) + \frac{\Phi_e}{R} d(Q_e L) + \frac{\Phi_m}{R} d(Q_m L) - \frac{M}{2} \frac{L}{R} \frac{dR^2}{R^2} \\ &+ \left(M \frac{L}{R} - \frac{\kappa A}{8\pi G_N} \frac{L}{R} - \frac{\Phi_e}{R} Q_e L - \frac{\Phi_m}{R} Q_m L\right) \frac{d(L^2/G_N)}{L^2/G_N} \end{aligned} \quad (2.31)$$

Dyonic AdS black holes extended first law is then implied by the holographic dictionary (2.25), (2.26), and (2.30) corresponds to the following thermodynamic first law in the CFT.

$$dE = TdS + \tilde{\Phi}_e d\tilde{Q}_e + \tilde{\Phi}_m d\tilde{Q}_m - pd\mathcal{V} + \mu dC \quad (2.32)$$

The chemical potential μ linked with the C central charge and the CFT field pressure p are found to be set via a detail comparison of the bulk and boundary first laws, which are given in equations (2.32) and (2.33), respectively.

$$\mu = \frac{1}{C}(E - TS - \tilde{\Phi}_e \tilde{Q}_e - \tilde{\Phi}_m \tilde{Q}_m), \quad p = \frac{1}{2} \frac{E}{\mathcal{V}} \quad (2.33)$$

The first equation is the Euler equation given in (2.23) with constant magnetic and electric charges and the later equation is the CFT equation of state (EOS). The first equation also implies that the C (or N^2) is proportional to the free energy in the grand canonical ensemble i.e. $F_{11} = E - TS - \tilde{\Phi}_e \tilde{Q}_e - \tilde{\Phi}_m \tilde{Q}_m = \mu C$.

At last, we provide clear expressions for the thermodynamic variables of charged dyonic black holes dual to CFT states. We introduce certain dimensional variables-

$$x = \frac{r_+}{L}, \quad y = \frac{q_e}{L}, \quad y = \Phi_e, \quad z = \frac{q_m}{L}, \quad z = \Phi_m \quad (2.34)$$

using the holographic dictionary, the entropy (2.9), electric and magnetic charge (2.11) and (2.12) for the electric and magnetic potential can be related to the variables in the CFT. (2.30)-

$$S = 4\pi Cx^2, \quad \tilde{Q}_e = 4Cy, \quad \tilde{\Phi}_e = \frac{y}{Rx}, \quad \tilde{Q}_m = 4Cz, \quad \tilde{\Phi}_m = \frac{z}{Rx} \quad (2.35)$$

where C is central charge and R is boundary radius .

2.3 Energy (E), temperature (T) and chemical potential (μ) for $(\tilde{\Phi}_e, \tilde{Q}_m)$

Using (2.7), (2.8),(2.14) the ADM mass M and the Hawking's temperature using (2.16) can be related by using (2.30), (2.35) to the CFT boundary energy E and temperature T as

$$E = \frac{2c(x^2(y^2 + 1) + x^4 + z^2)}{Rx}, \quad T = -\frac{x^2(y^2 - 1) - 3x^4 + z^2}{4\pi Rx^3} \quad (2.36)$$

The chemical potential μ can be written in x, y, z and R by using (2.33), (2.35) and (2.36) we get:-

$$\mu = -\frac{-x^2(3y^2 + 1) + x^4 + 4y^2 + z^2}{Rx} \quad (2.37)$$

2.4 Energy (E), Temperature (T) and chemical potential (μ) for $(\tilde{\Phi}_m, \tilde{Q}_e)$

Now for $\tilde{\Phi}_m$ and \tilde{Q}_e , using (2.7), (2.8), (2.14), the ADM mass M and the Hawking temperature using(2.18) can be linked to the CFT boundary energy E and temperature T by using (2.30) and (2.35) as:-

$$E = \frac{2c(x^4 + x^2(z^2 + 1) + y^2)}{Rx}, \quad T = -\frac{-3x^4 + x^2(z^2 - 1) + y^2}{4\pi Rx^3} \quad (2.38)$$

And the chemical potential μ can be written in terms of x, y, z and R by using (2.33), (2.35) and (2.38) and obtain:-

$$\mu = -\frac{x^4 - x^2(3z^2 + 1) + y^2 + 4z^2}{Rx} \quad (2.39)$$

2.5 Energy (E), Temperature (T) and chemical potential (μ) for $(\tilde{\Phi}_e, \tilde{\Phi}_m)$

Now for $\tilde{\Phi}_e$ and $\tilde{\Phi}_m$, using (2.7), (2.8), (2.14), the ADM mass M and the Hawking temperature using (2.20) can be co-related to the CFT boundary temperature and CFT boundary energy by using (2.30) and (2.35) as:-

$$E = \frac{2Cx(x^2 + y^2 + z^2 + 1)}{R}, \quad T = -\frac{-3x^2 + y^2 + z^2 - 1}{4\pi Rx} \quad (2.40)$$

The chemical potential μ can be written in terms of x, y, z and R by using (2.33), (2.35) and (2.40) and obtain:-

$$\mu = \frac{-x^4 + x^2(3y^2 + 3z^2 + 1) - 4(y^2 + z^2)}{Rx} \quad (2.41)$$

2.6 Energy (E), Temperature (T) and chemical potential (μ) for $(\tilde{Q}_e, \tilde{Q}_m)$

Now, for \tilde{Q}_e and \tilde{Q}_m , using (2.7), (2.8), (2.14), the ADM mass M and the Hawking's temperature using (2.21) can be correlated to the CFT boundary temperature and CFT energy at the boundary by using (2.30) and (2.35) as:-

$$E = \frac{2C(x^4 + x^2 + y^2 + z^2)}{Rx}, \quad T = -\frac{-3x^4 - x^2 + y^2 + z^2}{4\pi Rx^3} \quad (2.42)$$

The chemical potential μ can be written in terms of x, y, z and R by using (2.33), (2.35) and (2.42) and obtain:-

$$\mu_4 = -\frac{x^4 - x^2 + y^2 + z^2}{Rx} \quad (2.43)$$

3 Different types of ensembles in the CFT thermodynamics

We want to examine the different canonical and grand canonical ensembles of the CFT thermodynamics using the holographic AdS/CFT dictionary. There are five complementary variables in the CFT thermodynamics depiction for dyonic Anti-de-Sitter black holes, namely $(\tilde{\Phi}_e, \tilde{Q}_e)$, $(\tilde{\Phi}_m, \tilde{Q}_m)$, (T, S) , (p, \mathcal{V}) and (μ, C) . For the dyonic black holes, we will be considering the ensembles:-

$$\text{fixed } (\tilde{Q}_m, \tilde{\Phi}_e, p, C) : \quad F_1 \equiv E - TS - \tilde{\Phi}_e \tilde{Q}_e + p\mathcal{V} = \tilde{\Phi}_m \tilde{Q}_m + \mu C + p\mathcal{V} \quad (3.1a)$$

$$\text{fixed } (\tilde{Q}_m, \tilde{\Phi}_e, p, \mu) : \quad F_2 \equiv E - TS - \tilde{\Phi}_e \tilde{Q}_e + p\mathcal{V} - \mu C = \tilde{\Phi}_m \tilde{Q}_m + p\mathcal{V} \quad (3.1b)$$

$$\text{fixed } (\tilde{Q}_m, \tilde{\Phi}_e, \mathcal{V}, C) : \quad F_3 \equiv E - TS - \tilde{\Phi}_e \tilde{Q}_e = \tilde{\Phi}_m \tilde{Q}_m + \mu C \quad (3.1c)$$

$$\text{fixed } (\tilde{Q}_m, \tilde{\Phi}_e, \mathcal{V}, \mu) : \quad F_4 \equiv E - TS - \tilde{\Phi}_e \tilde{Q}_e - \mu C = \tilde{\Phi}_m \tilde{Q}_m \quad (3.1d)$$

$$\text{fixed } (\tilde{\Phi}_m, \tilde{Q}_e, p, C) : \quad F_5 \equiv E - TS + \tilde{\Phi}_m \tilde{Q}_m + p\mathcal{V} = \tilde{\Phi}_e \tilde{Q}_e + \mu C + p\mathcal{V} \quad (3.1e)$$

$$\text{fixed } (\tilde{\Phi}_m, \tilde{Q}_e, p, \mu) : \quad F_6 \equiv E - TS - \tilde{\Phi}_m \tilde{Q}_m + p\mathcal{V} - \mu C = \tilde{\Phi}_e \tilde{Q}_e + p\mathcal{V} \quad (3.1f)$$

$$\text{fixed } (\tilde{\Phi}_m, \tilde{Q}_e, \mathcal{V}, C) : \quad F_7 \equiv E - TS - \tilde{\Phi}_m \tilde{Q}_m = \tilde{\Phi}_e \tilde{Q}_e + \mu C \quad (3.1g)$$

$$\text{fixed } (\tilde{\Phi}_m, \tilde{Q}_e, \mathcal{V}, \mu) : \quad F_8 \equiv E - TS - \tilde{\Phi}_m \tilde{Q}_m - \mu C = \tilde{\Phi}_e \tilde{Q}_e \quad (3.1h)$$

$$\text{fixed } (\tilde{\Phi}_m, \tilde{\Phi}_e, p, C) : \quad F_9 \equiv E - TS - \tilde{\Phi}_m \tilde{Q}_m - \tilde{\Phi}_e \tilde{Q}_e + p\mathcal{V} = \mu C + p\mathcal{V} \quad (3.1i)$$

$$\text{fixed } (\tilde{\Phi}_m, \tilde{\Phi}_e, p, \mu) : \quad F_{10} \equiv E - TS - \tilde{\Phi}_m \tilde{Q}_m - \tilde{\Phi}_e \tilde{Q}_e - \mu C + p\mathcal{V} = p\mathcal{V} \quad (3.1j)$$

$$\text{fixed } (\tilde{\Phi}_m, \tilde{\Phi}_e, \mathcal{V}, C) : \quad F_{11} \equiv E - TS - \tilde{\Phi}_m \tilde{Q}_m - \tilde{\Phi}_e \tilde{Q}_e = \mu C \quad (3.1k)$$

$$\text{fixed } (\tilde{\Phi}_m, \tilde{\Phi}_e, \mathcal{V}, \mu) : \quad F_{12} \equiv E - TS - \tilde{\Phi}_m \tilde{Q}_m - \tilde{\Phi}_e \tilde{Q}_e + \mu C = 0 \quad (3.1l)$$

$$\text{fixed } (\tilde{Q}_m, \tilde{Q}_e, p, C) : \quad F_{13} \equiv E - TS + p\mathcal{V} = +\tilde{\Phi}_m \tilde{Q}_m + \tilde{\Phi}_e \tilde{Q}_e + \mu C + p\mathcal{V} \quad (3.1m)$$

$$\text{fixed } (\tilde{Q}_m, \tilde{Q}_e, p, \mu) : \quad F_{14} \equiv E - TS + p\mathcal{V} + \mu C = +\tilde{\Phi}_m \tilde{Q}_m + \tilde{\Phi}_e \tilde{Q}_e + p\mathcal{V} \quad (3.1n)$$

$$\text{fixed } (\tilde{Q}_m, \tilde{Q}_e, \mathcal{V}, C) : \quad F_{15} \equiv E - TS = \tilde{\Phi}_m \tilde{Q}_m + \tilde{\Phi}_e \tilde{Q}_e + \mu C \quad (3.1o)$$

$$\text{fixed } (\tilde{Q}_m, \tilde{Q}_e, \mathcal{V}, \mu) : \quad F_{16} \equiv E - TS - \mu C = \tilde{\Phi}_m \tilde{Q}_m + \tilde{\Phi}_e \tilde{Q}_e \quad (3.1p)$$

In the subsections carried on, we study the behaviours of different phases seen in the list ensembles mentioned above.

Table 1: Different ensembles and their results

Ensembles	Phase transitions shown
$(\tilde{Q}_m, \tilde{\Phi}_e, p, C)$	Nil phase transition
$(\tilde{Q}_m, \tilde{\Phi}_e, p, \mu)$	Nil phase transition
$(\tilde{Q}_m, \tilde{\Phi}_e, \mathcal{V}, C)$	Phase transition of first and second order
$(\tilde{Q}_m, \tilde{\Phi}_e, \mathcal{V}, \mu)$	Phase transition of zeroth order
$(\tilde{\Phi}_m, \tilde{Q}_e, p, C)$	Nil phase transition
$(\tilde{\Phi}_m, \tilde{Q}_e, p, \mu)$	Nil phase transition
$(\tilde{\Phi}_m, \tilde{Q}_e, \mathcal{V}, C)$	Phase transition of first and second order
$(\tilde{\Phi}_m, \tilde{Q}_e, \mathcal{V}, \mu)$	Phase transition of zeroth order
$(\tilde{\Phi}_m, \tilde{\Phi}_e, p, C)$	Nil phase transition
$(\tilde{\Phi}_m, \tilde{\Phi}_e, p, \mu)$	Nil phase transition
$(\tilde{\Phi}_m, \tilde{\Phi}_e, \mathcal{V}, C)$	Confinement and de-confinement phase transitions
$(\tilde{\Phi}_m, \tilde{\Phi}_e, \mathcal{V}, \mu)$	No free energy plot seen
$(\tilde{Q}_m, \tilde{Q}_e, p, C)$	Nil phase transition
$(\tilde{Q}_m, \tilde{Q}_e, p, \mu)$	Nil phase transition
$(\tilde{Q}_m, \tilde{Q}_e, \mathcal{V}, C)$	Phase transition of first and second order
$(\tilde{Q}_m, \tilde{Q}_e, \mathcal{V}, \mu)$	Phase transition of zeroth order

3.1 For the fixed $(\tilde{Q}_m, \tilde{\Phi}_e, \mathcal{V}, C)$ ensemble

Fixing the magnetic charge \tilde{Q}_m , an electric potential $\tilde{\Phi}_e$, volume of space \mathcal{V} and CFT central charge C . The Helmholtz free energy is-

$$F_3 \equiv E - TS - \tilde{\Phi}_e \tilde{Q}_e = -\frac{C(x^4 - x^2 + y^2 - 3z^2)}{Rx} \quad (3.2)$$

The first law CFT given in (2.32), by differentiating of F_3 we get

$$\begin{aligned} dF_3 &= dE - TdS - SdT - \tilde{\Phi}_e d\tilde{Q}_e - \tilde{Q}_e d\tilde{\Phi}_e \\ &= -SdT + \tilde{\Phi}_m d\tilde{Q}_m - \tilde{Q}_e d\tilde{\Phi}_e - pd\mathcal{V} + \mu C \end{aligned} \quad (3.3)$$

Hence, we can see in (3.3), that F_3 is static for the fixed $(T, \tilde{Q}_m, \tilde{\Phi}_e, \mathcal{V}, C)$. Let us explore how the free energy F_3 (3.2) behaves w.r.t to the temperature T (2.16) for different fixed $(T, \tilde{Q}_m, \tilde{\Phi}_e, \mathcal{V}, C)$ values. We preferable to grasp the idea that F_3 and T are the functions of $(T, \tilde{Q}_m, \tilde{\Phi}_e, \mathcal{V}, C, x)$. The volume \mathcal{V} is fixed by fixing the radius R . We write the temperature and Gibbs free energy as below after substituting the parameters $y = \tilde{\Phi}_e Rx$ and $z = \frac{\tilde{Q}_m}{4C}$ for the $\tilde{\Phi}_e$ as electric potential and \tilde{Q}_m as magnetic charge.

$$\begin{aligned} F_3 &= \frac{3\tilde{Q}_m^2}{16cRx} - \frac{cx(R^2\tilde{\Phi}_e^2 + x^2 - 1)}{R} \\ T &= -\frac{\frac{\tilde{Q}_m^2}{16c^2} + x^2(R^2\tilde{\Phi}_e^2 - 3x^2 - 1)}{4\pi Rx^3} \end{aligned} \quad (3.4)$$

As a result, we may parametrically display $F(T)$ free energy and temperature using x as a condition for fixed

$(T, \tilde{Q}_m, \tilde{\Phi}_e, \mathcal{V}, C)$. Since scale invariance has fixed the dependence of R , changing the value of R will only cause the plots to rescale each other. When we plot $F_3(T)$ (3.4) using various values of \tilde{Q}_m while maintaining $\tilde{\Phi}_e, C$ or $\tilde{\Phi}_e$ while maintaining \tilde{Q}_m, C or C while maintaining $\tilde{\Phi}_e, \tilde{Q}_m$ fixed, we will obtain a "swallowtail" behaviour linking three branches. However, this only occurs when all three of the following conditions are met: $\tilde{Q}_m < \tilde{Q}_m^{critical}$, $\tilde{\Phi}_e < \tilde{\Phi}_e^{critical}$ and $C > C^{critical}$.

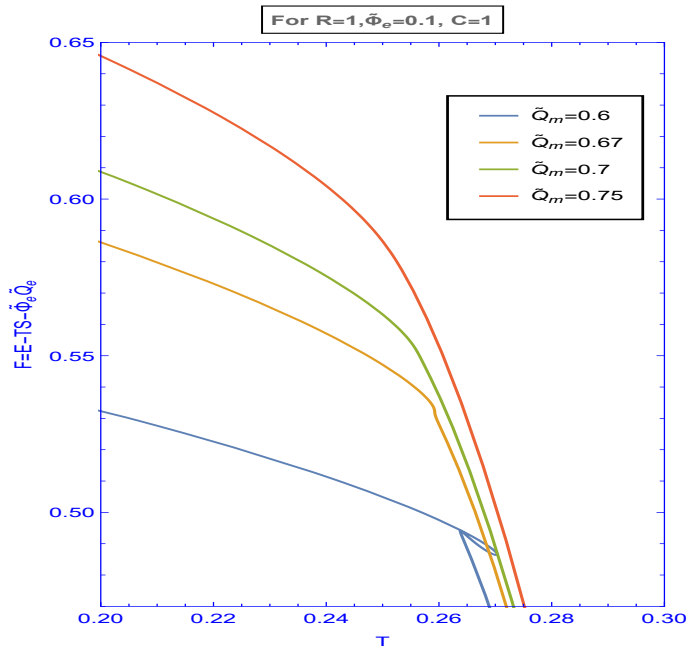


Figure 1: Plotting free energy F_3 vs. T for temperature for fixed $(\tilde{Q}_m, \tilde{\Phi}_e, \mathcal{V}, C)$ for various values of $\tilde{\Phi}_e$, when R, C, \tilde{Q}_m are kept constant.

For figure 1 we can see that the free energy F_3 being a function for temperature T for $\tilde{Q}_m < \tilde{Q}_m^{critical}$ (blue), $\tilde{Q}_m = \tilde{Q}_m^{critical}$ (orange) and $\tilde{Q}_m > \tilde{Q}_m^{critical}$ (green, red) while C, R and $\tilde{\Phi}_e$ are kept constant. Then the free energy F_3 shows a "swallow-tail" like structure when $\tilde{Q}_m < \tilde{Q}_m^{critical}$, a small kink structure when $\tilde{Q}_m = \tilde{Q}_m^{critical}$ and a monotonous smooth curve when $\tilde{Q}_m > \tilde{Q}_m^{critical}$. The value of x rises as T increases for each curve starting at $T = 0$. The Anti-de-Sitter black holes with tiny x are analog to the thermal states of the CFT with S/C being very small, which represents certain states having per degree of freedom low entropy, which can be observed from the entropy S formula. This low entropy state, free energy F_3 is the lowest, is only present around $T = 0$ for the swallowtail curve (blue). Up until a point where it intersects with itself, it still has the lowest free energy. Beyond this point, the curve's vertical branch is the location for a state with a high per degree of freedom entropy for the CFT, which is consistent with large x black holes. For various values of $\tilde{Q}_m < \tilde{Q}_m^{critical}$, there is a phase transition of first order at its self-intersection temperature between the low- and high-entropy states. The swallow-tail

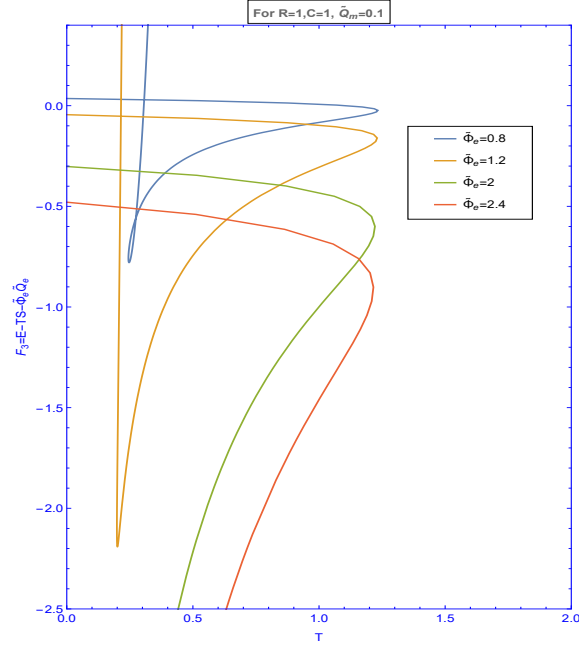


Figure 2: Plotting Free energy F_3 vs. T for temperature for fixed $(\tilde{Q}_m, \tilde{\Phi}_e, \mathcal{V}, C)$ for various values of \tilde{Q}_m , when $R, C, \tilde{\Phi}_e$ are kept constant.

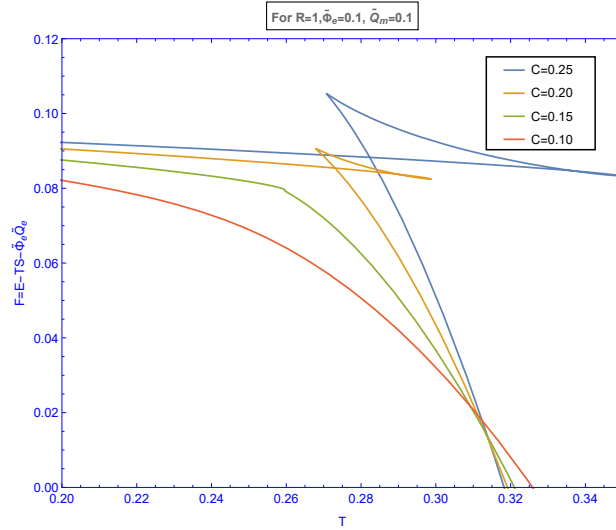


Figure 3: Plotting free energy F_3 vs T for temperature for fixed $(\tilde{Q}_m, \tilde{\Phi}_e, \mathcal{V}, C)$ for various values of C , when $R, \tilde{\Phi}_e, \tilde{Q}_m$ are kept constant.

shrinks as \tilde{Q}_m is raised, and it continues to shrink until $\tilde{Q}_m = \tilde{Q}_m^{critical}$, at which point it stays as a kink in the curve. At this $(\tilde{Q}_m^{crit}, T_{crit})$ turning point, it changes to a second order phase transition and is dependent on C and $\tilde{\Phi}_e$.

For Figure 2 we can observe the $F_3(T)$ graph for the free energy F_3 as a function for the temperature T for $\tilde{\Phi}_e < \tilde{\Phi}_e^{crit}$ (blue, orange) and $\tilde{\Phi}_e > \tilde{\Phi}_e^{crit}$ (green, red) while C, R, \tilde{Q}_m are kept fixed. The free energy curve here also for $\tilde{\Phi}_e < \tilde{\Phi}_e^{crit}$, it cut itself at a particular point. For $\tilde{\Phi}_e > \tilde{\Phi}_e^{crit}$ it doesn't come in contact with the same curve. It is a bit different from the figure 1 analysis. For each value of $\tilde{\Phi}_e < \tilde{\Phi}_e^{crit}$, we obtain a phase transition of first-order and the self-overlapping pressure seen between the low- and high- entropy states. We see different branches related to the black holes having small, intermediate, and large branches, namely three branches. The horizontal branch matches to the small black hole and the vertical branch relates to the large black hole respectively. For each value of $\tilde{\Phi}_e > \tilde{\Phi}_e^{crit}$ we see only two branches, one horizontal which is for the low entropy which corresponds to small black holes and a vertical branch which corresponds to large black holes.

We additionally take into account different CFT central charge C values while maintaining $\tilde{\Phi}_e, \tilde{Q}_m$, and R constant. Figure 3 displays graphs of $F(T)$ for the conditions $C < C^{crit}$ (blue), $C = C^{crit}$ (orange), and $C > C^{crit}$ (green, red). This exhibits behavior that is similar to that of the earlier plots. In other words, for $C > C^{crit}$, the plot shows phase transitions between degrees of freedom with low and high entropy. On $C = C^{crit}$, we obtain a phase transition of first order and a phase transition of second order in $C < C^{crit}$. Until the critical charge is achieved, and the first and second-order phase transition is detected, the temperature drops as we decrease the central charge.

When comparing the three figures, it can be seen that phase transitions happen for large central charges $C > C^{crit}$, but for small electric potentials $\tilde{\Phi}_e < \tilde{\Phi}_e^{crit}$ and magnetic charges $\tilde{Q}_m < \tilde{Q}_m^{crit}$. In figure 3, the phase transition also becomes less pronounced as C falls, in contrast to figures 1 and 2, where the phase transition becomes more pronounced as $\tilde{\Phi}_e$ and \tilde{Q}_m fall.

3.2 For the fixed $(\tilde{Q}_m, \tilde{\Phi}_e, \mathcal{V}, \mu)$ ensemble

Fixing the CFT's central charge C in the preceding ensemble. Here, we explore the results of fixing the corresponding μ as the chemical potential. The ensemble's proper free energy F_4 depends on $(\tilde{Q}_m, \tilde{\Phi}_e, \mathcal{V}, \mu)$.

$$F_4 \equiv E - TS - \tilde{\Phi}_e \tilde{Q}_e - \mu C = \tilde{\Phi}_m \tilde{Q}_m \quad (3.5)$$

By differentiating F_4 , we get:-

$$\begin{aligned} dF_4 &= dE - TdS - SdT - \tilde{\Phi}_e d\tilde{Q}_e - \tilde{Q}_e d\tilde{\Phi}_e - \mu dC - Cd\mu \\ dF_4 &= -SdT + \tilde{\Phi}_m d\tilde{Q}_m - \tilde{Q}_e d\tilde{\Phi}_e - pd\mathcal{V} - Cd\mu \end{aligned} \quad (3.6)$$

where we put dE from equation (2.32) and simplify. Therefore, for fixed values of $(T, \tilde{Q}_m, \tilde{\Phi}_e, \mathcal{V}, \mu)$, the free energy F_4 is stationary. This implies that, for the CFT, we are free to investigate a group of holographic CFT theories with various C as central charges. This

refers to a change in Λ as cosmological and G_N as Newton's constant in the corresponding theory of gravity. (3.5) can be written as

$$F_4 = \tilde{Q}_m \frac{z}{Rx}$$

where we have put $\tilde{\Phi}_m = \frac{z}{Rx}$. Now from (2.37) we solve it in terms of z to get $z = \sqrt{-\mu Rx + x^2(3y^2 + 1) - x^4 - 4y^2}$ and put it in the above equation and get

$$F_4 = \frac{\tilde{Q}_m \sqrt{-\mu Rx + x^2(3y^2 + 1) - x^4 - 4y^2}}{Rx} \quad (3.7)$$

Similarly for the temperature, we use (2.36) and put the value of $z = \sqrt{-\mu Rx + x^2(3y^2 + 1) - x^4 - 4y^2}$ to get:-

$$T = \frac{\mu Rx + 4(-x^2 y^2 + x^4 + y^2)}{4\pi Rx^3} \quad (3.8)$$

Representing the free energy F_4 (3.7) and T for temperature (3.8) as functions $F_4 = F_4(\tilde{Q}_m, \tilde{\Phi}_e, R, \mu, x)$ and $T = T(\tilde{\Phi}_e, R, \mu, x)$ using lastly $y = \tilde{\Phi}_e Rx$ and we get:-

$$F_4 = \frac{|\tilde{Q}_m| \sqrt{x \left(x^3 \left(3R^2 \tilde{\Phi}_e^2 - 1 \right) - 4R^2 \tilde{\Phi}_e^2 x - \mu R + x \right)}}{Rx} \quad (3.9)$$

$$T = \frac{x^3 \left(4 - 4R^2 \tilde{\Phi}_e^2 \right) + 4R^2 \tilde{\Phi}_e^2 x + \mu R}{4\pi Rx^2}$$

We observe that the absolute value of \tilde{Q}_m is there because the free energy cannot be negative.

We can display $F_4(T)$ for given values of $(\tilde{Q}_m, \tilde{\Phi}_e, R, \mu)$ shown in figure 4 using equation (3.7). At $\mu = 0$, the graph exhibits a qualitative change that can be seen (green curve). The free energy F_4 is single-valued for the temperature function for $\mu \leq 0$ (blue, orange, and green), which translates to a single phase transition in the CFT that is static under thermal variations. The free energy curve for $0 < \mu < \mu_{coin}$ (purple and red) has branches namely two that split $G = 0$ at T_1 and T_2 temperatures, where $T_2 \geq T_1$ corresponds to the root $f(x) = \tilde{\Phi}_e^2 x R^2 + \mu R + x^3 - x$. To solve this we take the two positive roots that are:-

$$x_1 = \frac{\sqrt[3]{6} (1 - i\sqrt{3}) (A)^{2/3} - 2 \cdot 2^{2/3} \sqrt[6]{3} (\sqrt{3} + 3i) R^4 \tilde{\Phi}_e^4 + 2 \cdot 2^{2/3} \sqrt[6]{3} (\sqrt{3} + 3i) R^2 \tilde{\Phi}_e^2}{12 \left(R^2 \tilde{\Phi}_e^2 - 1 \right) \sqrt[3]{A}}$$

$$x_2 = \frac{\sqrt[3]{6} (1 + i\sqrt{3}) (A)^{2/3} - 2 \cdot 2^{2/3} \sqrt[6]{3} (\sqrt{3} - 3i) R^4 \tilde{\Phi}_e^4 + 2 \cdot 2^{2/3} \sqrt[6]{3} (\sqrt{3} - 3i) R^2 \tilde{\Phi}_e^2}{12 \left(R^2 \tilde{\Phi}_e^2 - 1 \right) \sqrt[3]{A}}$$

where the value of A in the above equation is:-

$$A = \sqrt{3} \sqrt{R^2 \left(R^2 \tilde{\Phi}_e^2 - 1 \right)^3 \left(27\mu^2 \left(R^2 \tilde{\Phi}_e^2 - 1 \right) + 16R^4 \tilde{\Phi}_e^6 \right) + 9\mu R^5 \tilde{\Phi}_e^4 - 18\mu R^3 \tilde{\Phi}_e^2 + 9\mu R}$$

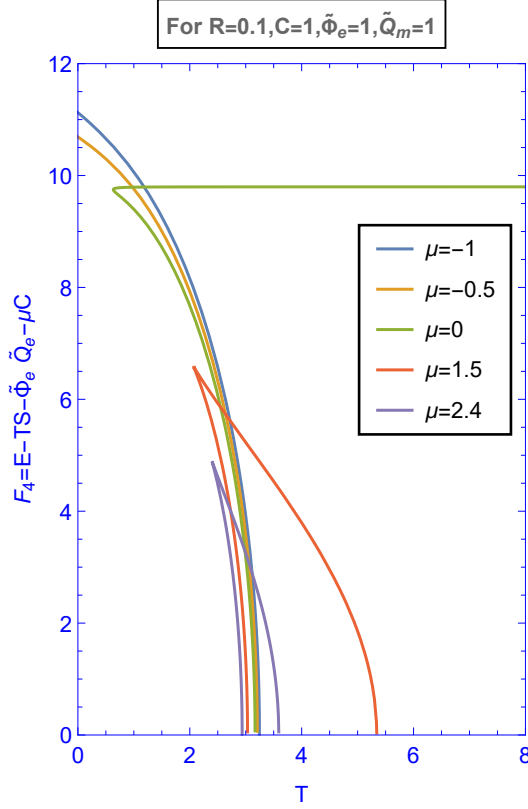


Figure 4: Plotting free energy F_4 vs T as temperature, we get the phase diagram for fixed $(\tilde{Q}_m, \tilde{\Phi}_e, R, \mu)$ ensemble. We set $R = 0.1$ and $\tilde{\Phi}_e = 1$ and $\tilde{Q}_m = 1$

Putting the value of the roots x_1 and x_2 in the temperature equation (3.7) we get the two temperatures namely T_1 and T_2 .

$$T_1 = \frac{144(B) \left(R\tilde{\Phi}_e - 3R^3\tilde{\Phi}_e^3 \right)^2 (A)^{2/3} + 432R\mu \left(1 - 3R^2\tilde{\Phi}_e^2 \right)^3 (A) - R^2\tilde{\Phi}_e^2 (B)^3}{12\pi R \left(1 - 3R^2\tilde{\Phi}_e^2 \right) \sqrt[3]{A} (B)^2} \quad (3.10)$$

where A and B are given as:-

$$A = 243\mu\tilde{\Phi}_e^4 R^5 - 162\mu\tilde{\Phi}_e^2 R^3 + 27\mu R + \sqrt{729R^2\mu^2 \left(1 - 3R^2\tilde{\Phi}_e^2 \right)^4 + 4 \left(-36R^4\tilde{\Phi}_e^4 + 21R^2\tilde{\Phi}_e^2 - 3 \right)^3}$$

$$B = 2^{2/3} \left(i\sqrt{3} + 1 \right) (A)^{2/3} + 6\sqrt[3]{2} \left(1 - i\sqrt{3} \right) \left(12R^4\tilde{\Phi}_e^4 - 7R^2\tilde{\Phi}_e^2 + 1 \right)$$

$$T_2 = \frac{144(B) \left(R\tilde{\Phi}_e - 3R^3\tilde{\Phi}_e^3 \right)^2 (A)^{2/3} + 432R\mu \left(1 - 3R^2\tilde{\Phi}_e^2 \right)^3 (A) - R^2\tilde{\Phi}_e^2 (B)^3 + (B)^3}{12\pi R \left(1 - 3R^2\tilde{\Phi}_e^2 \right) \sqrt[3]{A} (B)^2} \quad (3.11)$$

Similarly, the terms A and B above are

$$A = 243\mu\tilde{\Phi}_e^4 R^5 - 162\mu\tilde{\Phi}_e^2 R^3 + 27\mu R + \sqrt{729R^2\mu^2 \left(1 - 3R^2\tilde{\Phi}_e^2\right)^4 + 4 \left(-36R^4\tilde{\Phi}_e^4 + 21R^2\tilde{\Phi}_e^2 - 3\right)^3}$$

$$B = 2^{2/3} \left(1 - i\sqrt{3}\right) (A)^{2/3} + 12\sqrt[3]{-2} \left(12R^4\tilde{\Phi}_e^4 - 7R^2\tilde{\Phi}_e^2 + 1\right)$$

Further if we put $\mu = 0$, $\tilde{\Phi}_e = 0$ we get:-

$$T_1 = \frac{1}{\pi R}, \quad T_2 = 0 \quad (3.12)$$

The two temperatures T_1 and T_2 are at the same concurrence point, $\mu_{coin} = \frac{1.5}{4R}$ so that the concurrence point gives as $T_{coin} = \frac{0.868}{\pi R}$. We see that we do not get any plots of $F_4(T)$ when $\mu > \mu_{coin}$. So hence we only get the plots when $\mu < \mu_{coin}$

In Fig 4 using the red curve, the right crossing point T_2 , the variable x increases along the line of curve until it reaches the cusp at T_0 , and then decreases as proceeded down from the turning point to the intersection point at left T_1 . As a result, the phase CFT between the turning point or the cusp and T_2 is a phase of low entropy, while the state between the turning point and T_1 is a phase of high entropy. We can obtain the temperature of the stationary point T_0 as

$$\left(\frac{dT}{dx}\right)_\mu = 0, \quad \text{we get}$$

$$x_0 = \frac{12R^4\tilde{\Phi}_e^4 - 12R^2\tilde{\Phi}_e^2}{3^{2^{2/3}(R^2\tilde{\Phi}_e^2 - 1)} \sqrt[3]{108\mu R^5\tilde{\Phi}_e^4 - 216\mu R^3\tilde{\Phi}_e^2 + \sqrt{(108\mu R^5\tilde{\Phi}_e^4 - 216\mu R^3\tilde{\Phi}_e^2 + 108\mu R)^2 + 4(12R^4\tilde{\Phi}_e^4 - 12R^2\tilde{\Phi}_e^2)^3 + 108\mu R}}}$$

$$- \frac{\sqrt[3]{108\mu R^5\tilde{\Phi}_e^4 - 216\mu R^3\tilde{\Phi}_e^2 + \sqrt{(108\mu R^5\tilde{\Phi}_e^4 - 216\mu R^3\tilde{\Phi}_e^2 + 108\mu R)^2 + 4(12R^4\tilde{\Phi}_e^4 - 12R^2\tilde{\Phi}_e^2)^3 + 108\mu R}}}{6\sqrt[3]{2}(R^2\tilde{\Phi}_e^2 - 1)}$$

Putting it in temperature T we get,

$$T_0 = \frac{\left(R^2\tilde{\Phi}_e^2 - 1\right) \left(R\tilde{\Phi}_e^2 \left(9R \left(\sqrt{3}\sqrt{B}\mu - 4\sqrt[3]{6}\sqrt[3]{A}\mu\right) - 4\sqrt[3]{2}3^{5/6}\sqrt[3]{A}\sqrt{B} + 243\mu^2 R^2\right) - 9\mu \left(\sqrt{3}\sqrt{B} + 9\mu R\right)\right)}{2^{2/3}\pi^2 \left(-2\sqrt[3]{6}R^4\tilde{\Phi}_e^4 + 2\sqrt[3]{6}R^2\tilde{\Phi}_e^2 + A^{2/3}\right) \sqrt[3]{3\mu R^5\tilde{\Phi}_e^4 - 6\mu R^3\tilde{\Phi}_e^2 + \frac{\sqrt{B}}{\sqrt{3}} + 3\mu R}}$$

$$- \frac{\left(R^2\tilde{\Phi}_e^2 - 1\right) \left(R^5\tilde{\Phi}_e^6 \left(8 \ 6^{2/3} A^{2/3} - 36\sqrt[3]{6}\sqrt[3]{A}\mu R + 81\mu^2 R^2\right) + R^3\tilde{\Phi}_e^4 \left(8 \ 6^{2/3} A^{2/3} - 72\sqrt[3]{6}\sqrt[3]{A}\mu R + 243\mu^2 R^2\right)\right)}{2^{2/3}\pi^2 \left(-2\sqrt[3]{6}R^4\tilde{\Phi}_e^4 + 2\sqrt[3]{6}R^2\tilde{\Phi}_e^2 + A^{2/3}\right) \sqrt[3]{3\mu R^5\tilde{\Phi}_e^4 - 6\mu R^3\tilde{\Phi}_e^2 + \frac{\sqrt{B}}{\sqrt{3}} + 3\mu R}} \quad (3.13)$$

Where A and B are:-

$$A = 9\mu\tilde{\Phi}_e^4 R^5 - 18\mu\tilde{\Phi}_e^2 R^3 + 9\mu R + \sqrt{3} \sqrt{R^2 \left(R^2\tilde{\Phi}_e^2 - 1\right)^3 \left(16R^4\tilde{\Phi}_e^6 + 27R^2\mu^2\tilde{\Phi}_e^2 - 27\mu^2\right)}$$

$$B = R^2 \left(R^2\tilde{\Phi}_e^2 - 1\right)^3 \left(16R^4\tilde{\Phi}_e^6 + 27R^2\mu^2\tilde{\Phi}_e^2 - 27\mu^2\right)$$

When we look at the phase transitions in this ensemble, there is just one for $\mu \leq 0$, but if we look at $0 < \mu < \mu_{coin}$, we can find a change of phase that happens between the branches of low and high entropy. Because the free energy for the state of high-entropy is lowest for $T_0 < T < T_1$, this stage is favored thermodynamically in this area of observation. The high entropy phase ends at $T = T_1$, and then there is a phase transition of zeroth-order between the states of high and low entropy. The entropy state that is the lower one is the only existing phase for $T_1 < T < T_2$ and thus dominates the thermodynamic ensemble.

We can see that the phase transition of zeroth order could occur in either direction between the entropy states of high and low depends on whether the temperature is lowered or raised. The change of phase from the entropy states from high to the low is seen when the CFT temperature rises above $T = T_1$, since this temperature above, only the branch of low entropy remains, but this change is unusual because the entropy during the process it decreases, which violates the second law of thermodynamics. Otherside, the chage of phase from the different entropy states namely the low- to high occurs when temperature falls below $T = T_1$, and this change appears more advantageous thermodynamically because the entropy during the process increases.

3.3 For the fixed $(\tilde{Q}_e, \tilde{\Phi}_m, \mathcal{V}, C)$ ensemble

We take electric charge $\tilde{\Phi}_e$ and magnetic potential $\tilde{\Phi}_m$ for this ensemble. Here we take thermodynamic CFT volume \mathcal{V} and CFT central charge C . Hence, now the free energy for this ensemble is calculated as:-

$$F_7 = E - TS - \tilde{\Phi}_m \tilde{Q}_m = \frac{c(-x^4 + x^2(3z^2 + 1) + 3y^2 - 4z^2)}{Rx} \quad (3.14)$$

By using the first CFT law (2.32) the differential of F_7 gives

$$\begin{aligned} dF_7 &= dE - TdS - SdT - \tilde{\Phi}_m d\tilde{Q}_m - \tilde{Q}_m d\tilde{\Phi}_m \\ dF_7 &= -SdT + \tilde{\Phi}_e d\tilde{Q}_e - \tilde{Q}_m d\tilde{\Phi}_m - pd\mathcal{V} + \mu dC \end{aligned} \quad (3.15)$$

Hence, from (3.15) we can infer that F_7 is seen to be stationary at fixed $(T, \tilde{Q}_e, \tilde{\Phi}_m, \mathcal{V}, C)$. Let us now study the performance of the Helmholtz free energy F_7 w.r.t to the temperature T given for different values of the $(T, \tilde{Q}_e, \tilde{\Phi}_m, \mathcal{V}, C)$. Mostly it is useful to think of F_7 and T for the different values of $(T, \tilde{Q}_e, \tilde{\Phi}_m, \mathcal{V}, C, x)$ for the required practical purposes. R as the radius is used to fix the thermodynamic CFT volume \mathcal{V} . The Helmholtz free energy and the temperature are written by simplifying the above equation by putting the values of $y = \frac{\tilde{Q}_e}{4C}$ and $z = \tilde{\Phi}_m Rx$ and we get:-

$$F_7 = \frac{3\tilde{Q}_e^2}{16cRx} + \frac{c(R^2\tilde{\Phi}_m^2(3x^2 - 4)x - x^3 + x)}{R} \quad (3.16)$$

Similarly also in the expression of temperature from (2.38), we put the value of $y = \frac{\tilde{Q}_e}{4C}$ and $z = \tilde{\Phi}_m Rx$ and simplifying we get:-

$$T = -\frac{\frac{\tilde{Q}_e^2}{16c^2} + x^4(R^2\tilde{\Phi}_m^2 - 3) - x^2}{4\pi Rx^3} \quad (3.17)$$

By using the free energy expression (3.16) and the temperature (3.17), we can plot the parametric plot between the two. The resulting parametric plots are given below. As a

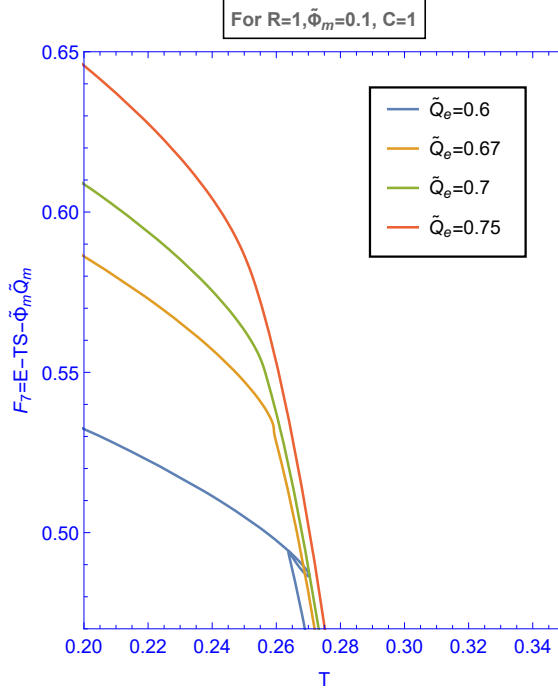


Figure 5: Plotting the free energy F_7 vs. temperature T and various phases for the fixed $(\tilde{\Phi}_m, \tilde{Q}_e, \mathcal{V}, C)$ ensemble. We set $R =$ and $C = 1$ and $\tilde{\Phi}_m = 0.1$

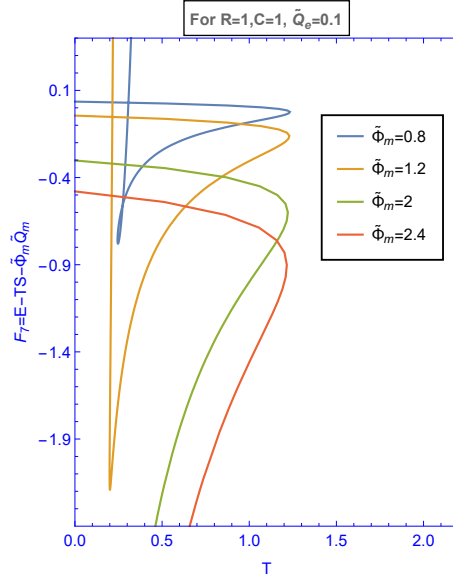


Figure 6: Plotting the free energy F_7 vs. temperature T and different phases for the fixed $(\tilde{\Phi}_m, \tilde{Q}_e, \mathcal{V}, C)$ ensemble. We set $R = 1$ and $\tilde{Q}_e = 0.1$ and $C = 1$

result, using x as a variable for the fixed $(T, \tilde{Q}_e, \tilde{\Phi}_m, \mathcal{V}, C)$, we can parametrically display

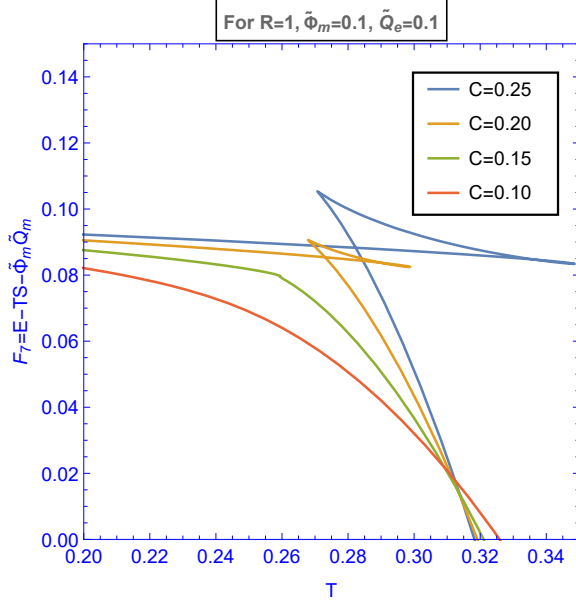


Figure 7: Plotting free energy F_7 vs. temperature T and different phases for the fixed $(\tilde{\Phi}_m, \tilde{Q}_e, \mathcal{V}, C)$ ensemble. We set $R = 1$ and $\tilde{\Phi}_m = 0.1$ and $\tilde{Q}_e = 0.1$ for different values of C

$F_7(T)$. The charts will only redraw themselves if the value of R is changed because the scale in variance has fixed the dependence of R . A "swallowtail" behaviour connecting three branches is obtained when we plot $F_7(T)$ using various values of $\tilde{\Phi}_m$ while maintaining \tilde{Q}_e , C (Figure 6), or \tilde{Q}_e while maintaining $\tilde{\Phi}_m$, C (Figure 5), or C while maintaining $\tilde{\Phi}_m$, \tilde{Q}_e fixed (Figure 7). But this only happens when all three of the following circumstances are true: Critical values for $\tilde{\Phi}_m < \tilde{\Phi}_m^{crit}$, $\tilde{Q}_e < \tilde{Q}_e^{crit}$ and $C > C_{crit}$.

For figure 5 we see that the free energy is plot parametrically with the temperature for $\tilde{Q}_e < \tilde{Q}_e^{crit}$ (blue), $\tilde{Q}_e = \tilde{Q}_e^{crit}$ (orange) and $\tilde{Q}_e > \tilde{Q}_e^{crit}$ (green, red) while keeping C , R and $\tilde{\Phi}_m$ constant. The Helmholtz free energy plot shows a "swallow tail" like structure when $\tilde{Q}_e < \tilde{Q}_e^{crit}$, a kink like structure when $\tilde{Q}_e = \tilde{Q}_e^{crit}$ and a smooth curve when $\tilde{Q}_e > \tilde{Q}_e^{crit}$. Value of x rises when T rises for each curve starting at $T = 0$. The black hole with tiny x is said to be analogous to the thermal states of the CFT with small S/C , which is used to denote states with a lower entropy per degree of freedom, as can be observed from the entropy formula. This low entropy state, which has the least free energy F_7 present around $T = 0$ for the "swallow tail" curve (blue). It still has the lowest free energy up to the degree where it overlaps itself. Beyond this threshold, a CFT state having per degree of freedom with increased entropy, which is consistent with big black holes, is located on the vertical branch of the curve. At the point of self-intersection for the temperature, there is a phase change of first-order between the entropy states of low- and high for various crucial value of $\tilde{Q}_e < \tilde{Q}_e^{crit}$. The "swallow tail" contracts when \tilde{Q}_e is raised, and it does so until $\tilde{Q}_e = \tilde{Q}_e^{crit}$, after which it just remains as a kink like structure. The change in the phase shifts to the order of two at this $(\tilde{Q}_e^{crit}, T_{crit})$ crucial point and becomes dependent on C and $\tilde{\Phi}_m$.

Figure 6 plots the free energy F_7 parametrically with temperature T for $\tilde{\Phi}_m < \tilde{\Phi}_m^{crit}$ (blue, orange) and $\tilde{\Phi}_m > \tilde{\Phi}_m^{crit}$ (green, red), all with fixed values for C , R , and \tilde{Q}_e . The free energy curve exhibits an intersection to itself here as well for $\tilde{\Phi}_m < \tilde{\Phi}_m^{crit}$ and a smooth curve for $\tilde{\Phi}_m > \tilde{\Phi}_m^{crit}$. The concepts are different from the analysis in figure 6. For each value of $\tilde{\Phi}_m < \tilde{\Phi}_m^{crit}$, we obtain a phase transition of first order of the self-matching pressure between the entropy states of low- and high. Here we see three branches which correspond to black holes having small, intermediate, and large graphs. The horizontal graphs relates to the small black hole and the vertical graph relates to the large black hole. For each value of $\tilde{\Phi}_m > \tilde{\Phi}_m^{crit}$ we see only two branches, one horizontal which is for the low entropy which corresponds to small black holes and a vertical branch which corresponds to large black holes.

While keeping $\tilde{\Phi}_m$, \tilde{Q}_e , and R constant, we also take varied values of C into consideration. For the circumstances $C < C_{crit}$ (blue), $C = C_{crit}$ (orange), and $C > C_{crit}$ (green, red), Figure 7 shows graphs of $F_7(T)$. This behaves in a manner reminiscent of the prior plots. To put it another way, the plot displays first-order phase transitions between degrees of freedom with entropy states for low and high for $C > C_{crit}$. At first, a phase transition single order and a phase transition second order in $C < C_{crit}$ and on $C = C_{crit}$ is seen respectively. As the central charge is reduced, the temperature decreases until the crucial value charge is reached and a second-order phase transition is observed. If the three figures are compared, it is clear that phase transitions only occur for big central charges $C > C_{crit}$ and do not occur for tiny electric potentials $\tilde{\Phi}_m < \tilde{\Phi}_m^{crit}$ or electric charges $\tilde{Q}_e < \tilde{Q}_e^{crit}$. In contrast to figures 6 and 5, where the phase transition becomes more prominent as $\tilde{\phi}_m$ and \tilde{Q}_e decline, the phase transition is similarly less pronounced in figure 7 as C decreases.

3.4 For the fixed $(\tilde{Q}_e, \tilde{\Phi}_m, \mathcal{V}, \mu)$ ensemble

Here, we study what happens when the appropriate chemical potential μ is fixed. The correct free energy of the ensemble $(\tilde{Q}_e, \tilde{\Phi}_m, \mathcal{V}, C)$ is:-

$$F_8 = E - TS - \tilde{\Phi}_m \tilde{Q}_m - \mu C = \frac{4Cy^2}{Rx} \quad (3.18)$$

By differentiating F_8 we get

$$\begin{aligned} dF_8 &= dE - TdS - SdT - \tilde{\Phi}_m d\tilde{Q}_m - \tilde{Q}_m d\tilde{\Phi}_m - \mu dC - Cd\mu \\ dF_8 &= -SdT - \tilde{Q}_m d\tilde{\Phi}_m + \tilde{\Phi}_m d\tilde{Q}_e - Cd\mu + pd\mathcal{V} \end{aligned} \quad (3.19)$$

where we put equation (2.32) and simplify. Hence for the fixed value of $(T, \tilde{\Phi}_m, \tilde{Q}_e, \mathcal{V}, \mu)$ the Helmholtz free energy F_8 is stationary. Then we put the value of $C = \frac{\tilde{Q}_e}{4y}$ we get,

$$F_8 = \frac{\tilde{Q}_e y}{Rx} \quad (3.20)$$

Now we solve the chemical potential μ (2.39) in terms of y to get

$$y = \sqrt{-\mu Rx - x^4 + x^2(3z^2 + 1) - 4z^2}$$

and put it on the free energy equation to get:-

$$F_8 = \frac{\tilde{Q}_e \sqrt{\mu R x - x^4 + x^2 (3z^2 + 1) - 4z^2}}{R x} \quad (3.21)$$

Now, we put the value of $z = \tilde{\Phi}_m R x$, then the free energy obtained will be:-

$$F_8 = \frac{\tilde{Q}_e \sqrt{x \left(x^3 \left(3R^2 \tilde{\Phi}_m^2 - 1 \right) - 4R^2 \tilde{\Phi}_m^2 x - \mu R + x \right)}}{R x} \quad (3.22)$$

Similarly, we work on the temperature by first incorporating it with

$$y = \sqrt{-\mu R x - x^4 + x^2 (3z^2 + 1) - 4z^2}$$

from solving (2.39) w.r.t y and then putting $z = \tilde{\Phi}_m R x$, so the temperature (2.38) is simplified with the required ensembles is:-

$$T = \frac{4 \left(-R^2 \tilde{\Phi}_m^2 x^4 + R^2 \tilde{\Phi}_m^2 x^2 + x^4 \right) + \mu R x}{4\pi R x^3} \quad (3.23)$$

Hence finally we plot parametrically the free energy F_8 and the temperature T . Hence

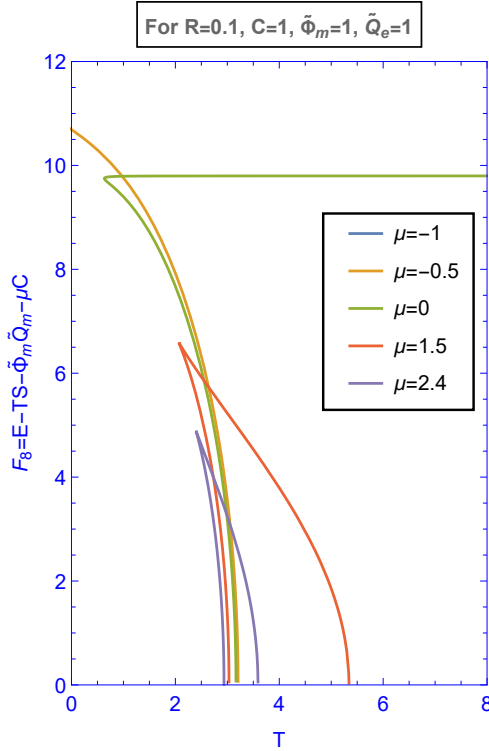


Figure 8: Plotting the free energy F_8 vs temperature T and observing various phase structures for the fixed $(\tilde{\Phi}_m, \tilde{Q}_e, \mathcal{V}, \mu)$ ensemble. We set $R = 0.1$ and $\tilde{\Phi}_m = 1$ and $\tilde{Q}_e = 1$

for a particular CFT, we are free to investigate a set of holographic CFT theories with

different chemical potential μ . This refers to a change in Λ and G_N in the corresponding gravity theory. We can write the free energy F_8 (3.22) and also the temperature T (3.23) as a function of $F_8 = F_8(\tilde{\Phi}_m, \tilde{Q}_e, R, \mu, x)$ and temperature $T = T(R, \mu, x)$. We see from the above formula that since the value of \tilde{Q}_e cannot be negative, so the absolute value is given. We can display the parametric plot for F_8 for different values of $(\tilde{\Phi}_m, \tilde{Q}_e, R, \mu)$. shown in the figure 8 using equation (3.22). At $\mu = 0$ in the graph, a qualitative change can be seen with the plot in the temperature given when we put $\mu = 0$. For $\mu \leq 0$ we can see that there is a single-value for the free energy which is a function of temperature, relating to the presence of a CFT single phase which is seen to be static under thermal fluctuations. For $0 \leq \mu \leq \mu_{coin}$ we see that the free energy graph has branches namely two, cutting the $F_8 \equiv 0$ lines at temperatures T_1 and T_2 where $T_2 \geq T_1$ which is calculated from the roots of the function which are positive: $x \left(x^3 \left(3R^2 \tilde{\Phi}_m^2 - 1 \right) - 4R^2 \tilde{\Phi}_m^2 x - \mu R + x \right) = 0$ The two roots are given as:-

$$x_1 = \frac{2^{2/3}(1-i\sqrt{3})(A)^{2/3} + 6\sqrt[3]{2}(1+i\sqrt{3})(12R^4\tilde{\Phi}_m^4 - 7R^2\tilde{\Phi}_m^2 + 1)}{12(1-3R^2\tilde{\Phi}_m^2)\sqrt[3]{A}} \quad (3.24)$$

$$x_2 = \frac{2^{2/3}(1+i\sqrt{3})(A)^{2/3} + 6\sqrt[3]{2}(1-i\sqrt{3})(12R^4\tilde{\Phi}_m^4 - 7R^2\tilde{\Phi}_m^2 + 1)}{12(1-3R^2\tilde{\Phi}_m^2)\sqrt[3]{A}} \quad (3.25)$$

where A is given as:-

$$A = \sqrt{729\mu^2 R^2 \left(1 - 3R^2\tilde{\Phi}_m^2\right)^4 + 4 \left(-36R^4\tilde{\Phi}_m^4 + 21R^2\tilde{\Phi}_m^2 - 3\right)^3 + 243\mu R^5\tilde{\Phi}_m^4 - 162\mu R^3\tilde{\Phi}_m^2 + 27\mu R} \quad (3.26)$$

Putting the value of the roots x_1 and x_2 in the temperature equation (3.23) we get the two temperatures namely T_1 and T_2 as:-

$$T_1 = \frac{144(A_0)(R\tilde{\Phi}_m - 3R^3\tilde{\Phi}_m^3)^2(B_0)^{2/3} + 432R\mu(1-3R^2\tilde{\Phi}_m^2)^3(B_0) - R^2\tilde{\Phi}_m^2(A_0)^3 + (A_0)^3}{B_1} \quad (3.27)$$

where A_0 and B_1 is given as

$$A_0 = 2^{2/3} \left(1 - i\sqrt{3}\right) (B_0)^{2/3} + 6\sqrt[3]{2} \left(i\sqrt{3} + 1\right) \left(12R^4\tilde{\Phi}_m^4 - 7R^2\tilde{\Phi}_m^2 + 1\right) \quad (3.28)$$

$$B_1 = 12\pi R \left(1 - 3R^2\tilde{\Phi}_m^2\right) \sqrt[3]{B_0} \left(2^{2/3} \left(1 - i\sqrt{3}\right) (B_0)^{2/3} + 6\sqrt[3]{2} \left(i\sqrt{3} + 1\right) \left(12R^4\tilde{\Phi}_m^4 - 7R^2\tilde{\Phi}_m^2 + 1\right)\right)^2 \quad (3.29)$$

$$T_2 = \frac{144(A_{01})(R\tilde{\Phi}_m - 3R^3\tilde{\Phi}_m^3)^2(B_0)^{2/3} + 432R\mu(1-3R^2\tilde{\Phi}_m^2)^3(B_0) - R^2\tilde{\Phi}_m^2(A_{01})^3 + (A_{01})^3}{B_2} \quad (3.30)$$

here A_{01} and B_2 is given as:-

$$A_{01} = 2^{2/3} \left(i\sqrt{3} + 1\right) (B_0)^{2/3} + 6\sqrt[3]{2} \left(1 - i\sqrt{3}\right) \left(12R^4\tilde{\Phi}_m^4 - 7R^2\tilde{\Phi}_m^2 + 1\right) \quad (3.31)$$

$$B_2 = 12\pi R \left(1 - 3R^2\tilde{\Phi}_m^2\right) \sqrt[3]{B_0} \left(2^{2/3} (i\sqrt{3} + 1) (B_0)^{2/3} + 6\sqrt[3]{2} (1 - i\sqrt{3}) \left(12R^4\tilde{\Phi}_m^4 - 7R^2\tilde{\Phi}_m^2 + 1\right)\right)^2 \quad (3.32)$$

Overall the value of B_0 for both T_1 and T_2 is

$$B_0 = 243\mu\tilde{\Phi}_m^4 R^5 - 162\mu\tilde{\Phi}_m^2 R^3 + 27\mu R + \sqrt{729R^2\mu^2 \left(1 - 3R^2\tilde{\Phi}_m^2\right)^4 + 4 \left(-36R^4\tilde{\Phi}_m^4 + 21R^2\tilde{\Phi}_m^2 - 3\right)^3} \quad (3.33)$$

Further if we put $\mu = 0$, $\tilde{\Phi}_m = 0$ we get:-

$$T_1 = \frac{1}{\pi R}, \quad T_2 = 0 \quad (3.34)$$

Further carrying on we notice that the two temperatures T_1 and T_2 are the same at the intersection point, $\mu_{coin} = \frac{1.5}{4R}$ so that the coincidence point gives as $T_{coin} = \frac{0.868}{\pi R}$. We noticed that we have not obtained any plot for $F_8(T)$ when $\mu > \mu_{coin}$. So only the plots when $\mu < \mu_{coin}$ are obtained.

In Fig 8, using the red curve, the significance of the x parameter grows along the line of curve up to the turning point at T_0 , and then lowers as it goes down from the turning point to the left coincidence point T_1 . As a result, the CFT state between the cusp and T_2 has less entropy, but the state between the turning point and T_1 has a elevated entropy. The temperature of the stationary point T_0 is calculated as

$$\left(\frac{dT}{dx}\right)_\mu = 0, \quad \text{we get}$$

$$x_0 = \frac{12R^4\tilde{\Phi}_m^4 - 12R^2\tilde{\Phi}_m^2}{3 \cdot 2^{2/3} (R^2\tilde{\Phi}_m^2 - 1) \sqrt[3]{108\mu R^5\tilde{\Phi}_m^4 - 216\mu R^3\tilde{\Phi}_m^2 + \sqrt{(108\mu R^5\tilde{\Phi}_m^4 - 216\mu R^3\tilde{\Phi}_m^2 + 108\mu R)^2 + 4(12R^4\tilde{\Phi}_m^4 - 12R^2\tilde{\Phi}_m^2)^3 + 108\mu R}} + \sqrt[3]{108\mu R^5\tilde{\Phi}_m^4 - 216\mu R^3\tilde{\Phi}_m^2 + \sqrt{(108\mu R^5\tilde{\Phi}_m^4 - 216\mu R^3\tilde{\Phi}_m^2 + 108\mu R)^2 + 4(12R^4\tilde{\Phi}_m^4 - 12R^2\tilde{\Phi}_m^2)^3 + 108\mu R}}}{6\sqrt[3]{2}(R^2\tilde{\Phi}_m^2 - 1)}$$

Putting it in temperature T we get,

$$T_0 = \frac{(R^2\tilde{\Phi}_m^2 - 1) \left(R^5(-36A_3 + 81R^2\mu^2)\tilde{\Phi}_m^6 - R^3(-72A_3 + 243R^2\mu^2)\tilde{\Phi}_m^4 + R \left(-4\sqrt[3]{23^{5/6}\sqrt{A_2}\sqrt[3]{A_1} + 243R^2\mu^2 + 9R(\sqrt{3}\mu\sqrt{A_2} - 4\sqrt[3]{6}\mu\sqrt[3]{A_1}) \right) \tilde{\Phi}_m^2 - 9\mu(9R\mu + \sqrt{3}\sqrt{A_2}) \right)}{B} \quad (3.35)$$

where the value of A_1 , A_2 , A_3 and B is given as

$$A_1 = 9\mu\tilde{\Phi}_m^4 R^5 - 18\mu\tilde{\Phi}_m^2 R^3 + 9\mu R + \sqrt{3} \sqrt{R^2 \left(R^2\tilde{\Phi}_m^2 - 1 \right)^3 \left(16R^4\tilde{\Phi}_m^6 + 27R^2\mu^2\tilde{\Phi}_m^2 - 27\mu^2 \right)} \quad (3.36)$$

$$A_2 = R^2 \left(R^2\tilde{\Phi}_m^2 - 1 \right)^3 \left(16R^4\tilde{\Phi}_m^6 + 27R^2\mu^2\tilde{\Phi}_m^2 - 27\mu^2 \right) \quad (3.37)$$

$$A_3 = \sqrt[3]{6}R\mu\sqrt[3]{A_1} + 8 \cdot 6^{2/3} \left(9\mu\tilde{\Phi}_m^4 R^5 - 18\mu\tilde{\Phi}_m^2 R^3 + 9\mu R + \sqrt{3}\sqrt{A_2} \right)^{2/3} \quad (3.38)$$

$$B = 2^{2/3}\pi^3 \sqrt[3]{3\mu\tilde{\Phi}_m^4 R^5 - 6\mu\tilde{\Phi}_m^2 R^3 + 3\mu R + \frac{\sqrt{A_2}}{\sqrt{3}}} \left(\left(9\mu\tilde{\Phi}_m^4 R^5 - 18\mu\tilde{\Phi}_m^2 R^3 + 9\mu R + \sqrt{3}\sqrt{A_2} \right)^{2/3} - 2\sqrt[3]{6}R^4\tilde{\Phi}_m^4 + 2\sqrt[3]{6}R^2\tilde{\Phi}_m^2 \right)^2 \quad (3.39)$$

There is one phase transition in this ensemble for $\mu \leq 0$, but if we look at $0 < \mu < \mu_{coin}$, we can identify a change of phase that occurs between both the branches of low and high entropy. The high-entropy state of the free energy decreases as we see and increase in T_0 . The change in phase from the entropy state of high to low occurs when the temperature of the CFT state exceeds $T = T_1$, because crossing this temperature, only the branch having lesser entropy survives, but this change is pretty unusual because the entropy's value lessens quite upto an extent during the process, which violates the law of thermodynamics, precisely the second. The change of phase from the entropy values of low- to high, occurs when the value of temperature reduces below $T = T_1$, and this transition appears to be more thermodynamically preferable because the entropy rises during the process.

3.5 For the fixed $(\tilde{\Phi}_e, \tilde{\Phi}_m, \mathcal{V}, C)$ ensemble

Here we study what happens when we fix the potentials $\tilde{\Phi}_e, \tilde{\Phi}_m$ as well as the central charge C making it an ensemble such like $(\tilde{\Phi}_e, \tilde{\Phi}_m, \mathcal{V}, C)$. Therefore the Gibbs energy namely as F_{11} can be calculated as follows:-

$$F_{11} = E - TS - \tilde{\Phi}_e \tilde{Q}_e - \tilde{\Phi}_m \tilde{Q}_m = \mu C \quad (3.40)$$

The CFT first law in (2.32) and by differentiating F_{11} is given as:-

$$\begin{aligned} dF_{11} &= dE - TdS - SdT - \tilde{\Phi}_e d\tilde{Q}_e - \tilde{Q}_e d\tilde{\Phi}_e - \tilde{\Phi}_m d\tilde{Q}_m - \tilde{Q}_m d\tilde{\Phi}_m \\ dF_{11} &= -SdT - \tilde{Q}_e d\tilde{\Phi}_e - \tilde{Q}_m d\tilde{\Phi}_m + p\mathcal{V} + \mu dC \end{aligned} \quad (3.41)$$

From equation (3.41) we get that F_{11} is stationary for $(\tilde{\Phi}_e, \tilde{\Phi}_m, \mathcal{V}, C)$. Writing the free energy $F_{11} = \mu C$ by putting the value of μ from (2.41) and then in the language of $\tilde{\Phi}_e$ and $\tilde{\Phi}_m$ using the formulas $y = \tilde{\Phi}_e R x$ and $z = \tilde{\Phi}_m R x$. Hence we get the Gibbs free energy as:-

$$F_{11} = \frac{cx \left(-4R^2 \left(\tilde{\Phi}_e^2 + \tilde{\Phi}_m^2 \right) + x^2 \left(3R^2 \left(\tilde{\Phi}_e^2 + \tilde{\Phi}_m^2 \right) - 1 \right) + 1 \right)}{R} \quad (3.42)$$

We also write the temperature in the same form by using (2.40) and the formula $y = \tilde{\Phi}_e R x$ and $z = \tilde{\Phi}_m R x$ of ensembles as the free energy, We get:-

$$T = \frac{1 - x^2 \left(R^2 \left(\tilde{\Phi}_e^2 + \tilde{\Phi}_m^2 \right) - 3 \right)}{4\pi R x} \quad (3.43)$$

We plot the parametric plot between Gibbs free energy F_{11} and Temperature T keeping central charge C and magnetic potential $\tilde{\Phi}_m$ constant, we get a plot and it is given below:-

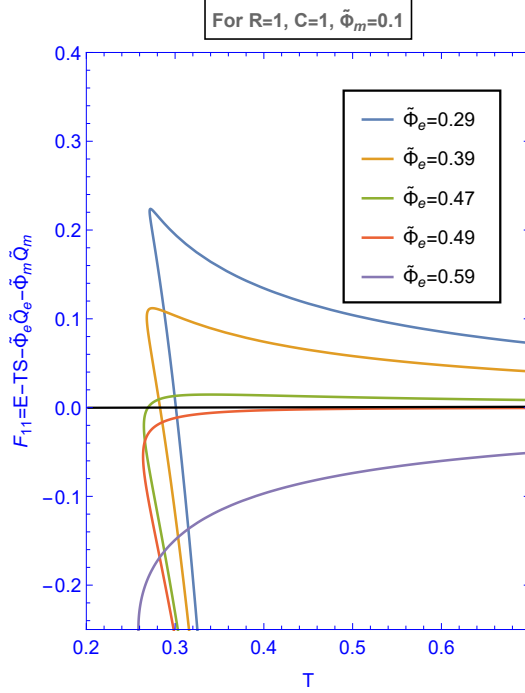


Figure 9: Plotting the free energy F_{11} vs. temperature T and various phase graphs for the fixed $(\tilde{\Phi}_m, \tilde{\Phi}_e, p, \mu)$ ensemble. We set $R = 1$ and $C = 1$ and $\tilde{\Phi}_m = 0.1$ and for different values of p

As seen in figure 9, this enables us to parametrically depict the free energy $F_{11}(T)$ using x parameter for the ensemble at fixed $(\tilde{\Phi}_e, \tilde{\Phi}_m, R, C)$. Different behaviour is portrayed on the $F_{11} - T$ plot crossing and staying below a specific crucial value of potential $\tilde{\Phi}_m^{crit}$. While $F_{11} \leq 0$ and the graph crosses the F_{11} axis for $\tilde{\Phi}_m \geq \tilde{\Phi}_m^{crit}$ (red and purple), we obtain a single value of free energy with the temperature as its function. In contrast, the free energy curve for $\tilde{\Phi}_m < \tilde{\Phi}_m^{crit}$ (blue, orange, and green) has an higher and lower branch that seems to converge at a turning point or cusp, representing, small black holes corresponding to low entropy and the big black holes corresponding to high entropy states. The temperature reaches a minimum value for the function of x i.e.

$$\left(\frac{dT}{dx}\right) = 0, \implies x_{cusp} = \frac{1}{\sqrt{-R^2\tilde{\Phi}_e^2 - R^2\tilde{\Phi}_m^2 + 3}}$$

Putting the value of x in (3.43) we get the minimum attained temperature as:-

$$T_{cusp} = \frac{\sqrt{3 - R^2(\tilde{\Phi}_e^2 + \tilde{\Phi}_m^2)}}{2\pi R} \quad (3.44)$$

According to the green curve in Figure 9, we see a change of phase of the order of one which is indicated by the lower branch's free energy changing sign at $F_{11} = 0$. While the "confined" state is thermodynamically favoured when $F_{11} > 0$, the huge entropy "deconfined" state

dominates the ensemble at $F_{11} < 0$. These phase transitions between (de)confinement and huge black holes in the AdS space and the AdS space-time with thermal radiation [39, 50] are analogous to a generalized transition of the Hawking Page phase. Although the Hawking page transition was first identified for charged Anti-de-Sitter Schwarzschild black holes [39], it also occurs for uncharged black holes in the AdS spacetime and is dependent on the electric potential [51].

3.6 For the fixed $(\tilde{\Phi}_e, \tilde{\Phi}_m, \mathcal{V}, \mu)$ ensemble

Here we take into consideration, if we set electric potential $\tilde{\Phi}_e$ and magnetic potential $\tilde{\Phi}_m$ constant instead of the charges then we get the grand canonical ensembles at fixed $(\tilde{\Phi}_e, \tilde{\Phi}_m, \mathcal{V}, \mu)$ ensembles. This is calculated as:-

$$F_{12} \equiv E - TS - \tilde{\Phi}_e \tilde{Q}_e - \tilde{\Phi}_m \tilde{Q}_m - \mu C = 0 \quad (3.45)$$

Using the equation (2.32), the differential of F_{12} can be expressed as:-

$$\begin{aligned} dF_{12} &= dE - TdS - SdT - \tilde{\Phi}_e d\tilde{Q}_e - \tilde{Q}_e d\tilde{\Phi}_e - \tilde{\Phi}_m d\tilde{Q}_m - \tilde{Q}_m d\tilde{\Phi}_m - \mu dC - Cd\mu \\ dF_{12} &= -SdT - \tilde{Q}_e d\tilde{\Phi}_e - \tilde{Q}_m d\tilde{\Phi}_m - Cd\mu + pd\mathcal{V} \end{aligned} \quad (3.46)$$

Since the free energy F_{12} is obtained as zero in this ensemble we cannot plot out F_{12} free energy versus temperature T . So, there is no parametric plot for this ensemble. Thus there is no study for criticality or phase transition.

3.7 For the fixed $(\tilde{Q}_e, \tilde{Q}_m, \mathcal{V}, C)$ ensemble

Here, we fixed both the electric charges \tilde{Q}_e, \tilde{Q}_m like before but this time we fixed the CFT's central charge C and obtained the ensemble $(\tilde{Q}_e, \tilde{Q}_m, \mathcal{V}, C)$. Therefore now the free energy is calculated as:-

$$F_{15} \equiv E - TS = \tilde{\Phi}_e \tilde{Q}_e + \tilde{\Phi}_m \tilde{Q}_m + \mu C \quad (3.47)$$

By differentiating F_{15} it can be expressed as:-

$$\begin{aligned} dF_{15} &= dE - TdS - SdT \\ dF_{15} &= -SdT + \tilde{\Phi}_e d\tilde{Q}_e + \tilde{\Phi}_m d\tilde{Q}_m + pd\mathcal{V} - \mu dC \end{aligned} \quad (3.48)$$

using equation (2.32) above we can see that the free energy F_{15} is static for the fixed $(T, \tilde{Q}_e, \tilde{Q}_m, \mathcal{V}, C)$ ensembles. Hence this is the correct expression. We write equation (3.47) by using (2.42), (2.9), in a direction containing \tilde{Q}_e, \tilde{Q}_m by taking values from the relation $y = \frac{\tilde{Q}_e}{4C}$ and $z = \frac{\tilde{Q}_m}{4C}$, so we get:-

$$F_{15} = \frac{3(\tilde{Q}_e^2 + \tilde{Q}_m^2)}{16cRx} + \frac{c(x - x^3)}{R} \quad (3.49)$$

Similarly, the temperature T (??) can be written using the same logic, so we get:-

$$T = -\frac{-16c^2x^2(3x^2 + 1) + \tilde{Q}_e^2 + \tilde{Q}_m^2}{64\pi c^2 R x^3} \quad (3.50)$$

As a result, using x as a variable for the fixed $(T, \tilde{Q}_m, \tilde{Q}_e, \mathcal{V}, C)$, we may parametrically show $F_{15}(T)$. The charts will only redraw themselves if the value of R changes because of scale invariance that has fixed the dependence of R . When we graph $F_{15}(T)$ using multiple quantities of \tilde{Q}_e while maintaining $\tilde{Q}_e m$ and C or \tilde{Q}_m while maintaining \tilde{Q}_e and C or C while maintaining \tilde{Q}_e and \tilde{Q}_m fixed, we obtain a *swallowtail* like structure. But only under the following three circumstances does this happen: Critical values include: $\tilde{Q}_e < \tilde{Q}_e^{critical}$, $\tilde{Q}_m < \tilde{Q}_m^{critical}$ and $C > C^{critical}$.

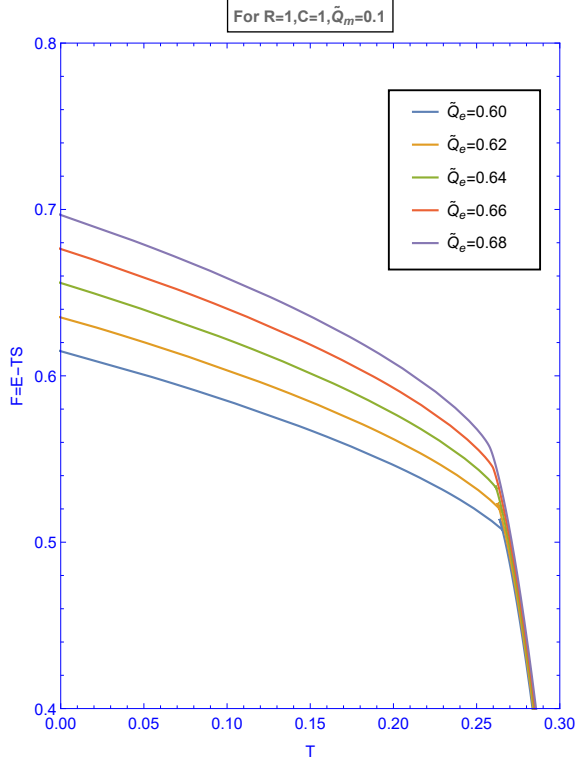


Figure 10: We plot the free energy F_{15} vs. temperature T and view the phase diagram for the fixed $(\tilde{Q}_m, \tilde{Q}_e, \mathcal{V}, C)$ ensemble. We set $R = 1$ and $C = 1$ and $\tilde{Q}_m = 0.1$ for different values of \tilde{Q}_e

Figure 10 is plotting parametrically the free energy F_{15} with respect to the temperature using x as a variable for the $\tilde{Q}_e < \tilde{Q}_e^{crit}$ system (blue), $\tilde{Q}_e = \tilde{Q}_e^{crit}$ (orange) and $\tilde{Q}_e > \tilde{Q}_e^{crit}$ (green, red, purple) keeping C , R , and \tilde{Q}_m constant. When $\tilde{Q}_e < \tilde{Q}_e^{critical}$, the free energy behaves in a manner resembling a *swallow tail*, a structure that resembles a kink when $\tilde{Q}_e = \tilde{Q}_e^{crit}$. Now, When $\tilde{Q}_e > \tilde{Q}_e^{crit}$, there is a smooth, monotonous curve. For each curve starting at $T = 0$, the variable x increases in value as T rises. It is seen from the entropy S formula, the black holes in AdS with minuscule x are analogous to the thermal states of the thermal CFT with lower S/C , where per degree of freedom, the states has low entropy. For the swallowtail like structure curve (blue), the entropy with a low value, which has the minimum free energy F_{15} , is only present around $T = 0$. It maintains the minimum free energy up to a certain point where it meets with itself. After crossing this part, a CFT

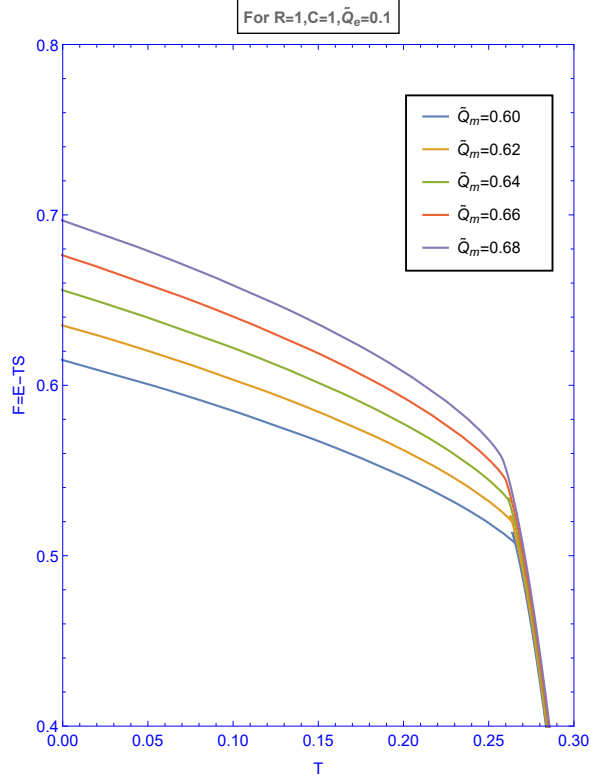


Figure 11: Plotting the free energy F_{15} vs. temperature T and viewing the phase graphs for the fixed $(\tilde{Q}_m, \tilde{Q}_e, \mathcal{V}, C)$ ensemble. We set $R = 1$ and $C = 1$ and $\tilde{Q}_e = 0.1$ for different values of \tilde{Q}_m

state where per degree of freedom has and elevated entropy, which is consistent with big x black holes, is located on the curve having a vertical branch. There is a phase transition in the order of first between the entropy states of low- and high at the self-coincidence temperature for certain values of $\tilde{Q}_e < \tilde{Q}_e^{crit}$. The *swallow tail* contracts as \tilde{Q}_e is increased and continues to contract until $\tilde{Q}_e = \tilde{Q}_e^{crit}$, after which it ceases to contract and remains as a kink like structure in the graph. The change in phase becomes second order and is dependent on C and \tilde{Q}_m at this $(\tilde{Q}_e^{crit}, T_{crit})$ critical point.

Figure 11 plots the free energy (3.49) with respect to the temperature T parametrically (3.50) for $\tilde{Q}_m > \tilde{Q}_m^{crit}$ (green, red, purple), $\tilde{Q}_m = \tilde{Q}_m^{crit}$ (orange), and $\tilde{Q}_m < \tilde{Q}_m^{crit}$ (blue), while holding C , R , and \tilde{Q}_e constant. Additionally, the free energy curve for \tilde{Q}_m has a *swallow tail* like behavior. It displays a kink like structure for $\tilde{Q}_m = \tilde{Q}_m^{crit}$ and a monotonous smooth curve for $\tilde{Q}_m > \tilde{Q}_m^{crit}$. Most of the concepts are the same as the analysis in figure 10. We find a change in phase of the self-coincidence pressure between the entropy states of low- and high for each value of $\tilde{Q}_m < \tilde{Q}_m^{crit}$. As the value of \tilde{Q}_m rises, the *swallow-tail* shrinks in size, and this process continues until we hit $\tilde{Q}_m = \tilde{Q}_m^{crit}$. At this specific critical point, or $(\tilde{Q}_m^{crit}, T_{crit})$, the change of phase transforms into a phase transition of second order that depends on C and \tilde{Q}_e .

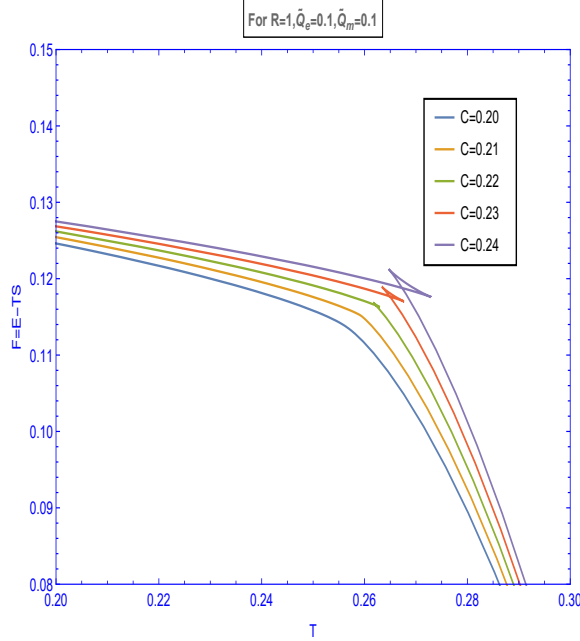


Figure 12: Plotting the free energy F_{15} vs. temperature T and viewing the phase graph for the fixed $(\tilde{Q}_m, \tilde{Q}_e, \mathcal{V}, C)$ ensemble. We set $R = 1$ and $\tilde{Q}_m = 0.1$ and $\tilde{Q}_e = 0.1$ for different values of C

In addition, while keeping \tilde{Q}_e , \tilde{Q}_m and R constants, we consider various values of C . Figure 12 shows graphs of $F_{15}(T)$ for the values of $C = C_{crit}$ (orange), $C > C_{crit}$ (green, red, purple) and $C < C_{crit}$ (blue). This behaves in a manner reminiscent of the prior plots. In other words, the graphic depicts phase changes between degrees of freedom with lower and higher values of entropy for $C > C_{crit}$. We find a change of phase of the first order and a change of phase of second order on the quantum point which is critical C_{crit} . The temperature plunges down as we decrease the CFT's central charge up until the critical charge is reached and a phase change of second order is observed.

When the three figures are compared, it is clear that phase transitions only occur for big central charges, or $C > C_{crit}$, but not for small electric charges $\tilde{Q}_e < \tilde{Q}_e^{crit}$ or for the magnetic charges $\tilde{Q}_m < \tilde{Q}_m^{crit}$. In contrast to figures 10 and 11, where the phase transition gets more prominent as \tilde{Q}_e and \tilde{Q}_m decrease, the phase transition likewise becomes less pronounced as C falls in figure 12

3.8 For the fixed $(\tilde{Q}_e, \tilde{Q}_m, \mathcal{V}, \mu)$ ensemble

We try to fix the electric charge \tilde{Q}_e and magnetic charges \tilde{Q}_m as well as the chemical potential μ and obtaining the ensemble $(\tilde{Q}_e, \tilde{Q}_m, \mathcal{V}, \mu)$. Hence, the Gibbs energy is obtained as below:-

$$F_{16} \equiv E - TS - \mu C = \tilde{\Phi}_e \tilde{Q}_e + \tilde{\Phi}_m \tilde{Q}_m = \frac{4C(y^2 + z^2)}{Rx} \quad (3.51)$$

After differentiating F_{16} we can write it as:-

$$\begin{aligned} dF_{16} &= dE - TdS - SdT - \mu dC - Cd\mu \\ dF_{16} &= -SdT - Cd\mu + \tilde{\Phi}_e d\tilde{Q}_e + \tilde{\Phi}_m d\tilde{Q}_m - p\mathcal{V} \end{aligned} \quad (3.52)$$

Expressing the free energy F_{16} with respect to the required ensemble, we need to incorporate the chemical potential μ from (2.43) by solving it for $C = \frac{\sqrt{-\tilde{Q}_e^2 - \tilde{Q}_m^2}}{4\sqrt{\mu R x + x^4 - x^2}}$ where we had to put $y = \frac{\tilde{Q}_e}{4C}, z = \frac{\tilde{Q}_m}{4C}$ in the μ equation and then putting it in the free energy equation we get:-

$$F_{16} = -\frac{\sqrt{-\tilde{Q}_e^2 - \tilde{Q}_m^2} \sqrt{x(\mu R + x^3 - x)}}{Rx} \quad (3.53)$$

We obtain the temperature (2.42) for this ensemble by incorporating the chemical potential (2.43) for $C = \frac{\sqrt{-\tilde{Q}_e^2 - \tilde{Q}_m^2}}{4\sqrt{\mu R x + x^4 - x^2}}$ and get:-

$$T = \frac{\mu + \frac{4x^3}{R}}{4\pi x^2} \quad (3.54)$$

where we have used $y = \frac{\tilde{Q}_e}{4C}, z = \frac{\tilde{Q}_m}{4C}$. Using the free energy F_{16} and the temperature T , we plot the parametric plot keeping \tilde{Q}_e, \tilde{Q}_m constant and obtain graphs for various values of μ . Equation (3.53) can be used to depict $F_{16}(T)$ parametrically for specified values

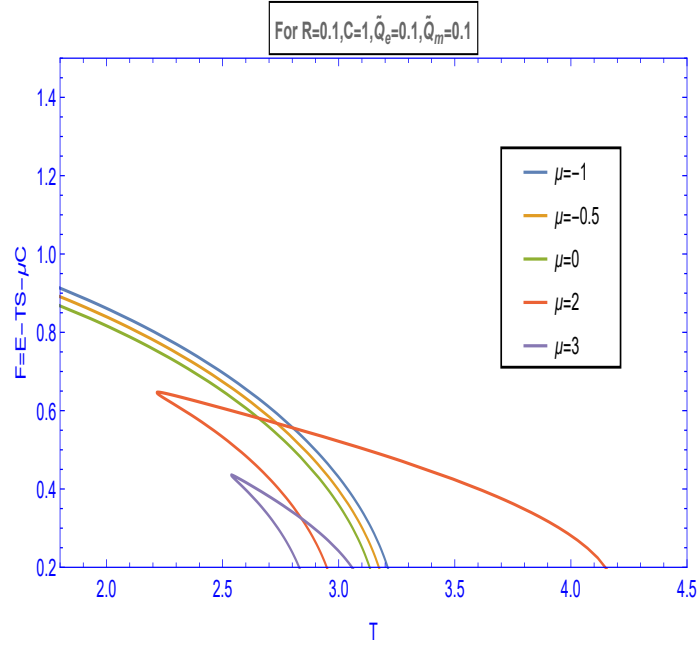


Figure 13: Plotting free energy F_{11} vs. temperature T and observing phase graphs for the fixed $(\tilde{Q}_m, \tilde{Q}_e, \mathcal{V}, \mu)$ ensemble. We set $R = 0.1$ and $C = 1$ and $\tilde{Q}_m = 0.1$ and $\tilde{Q}_e = 0.1$ for different values of μ

of $(\tilde{Q}_m, \tilde{Q}_e, R, \mu)$ illustrated in figure 13. The graph displays a noticeable characteristics

change at $\mu = 0$ (green curve). For $\mu \leq 0$ (blue, orange, and green), we see the free energy for the function of temperature is of only one-value, relating to a single change of phase in the CFT that is quite steady under thermal changes. At temperatures T_1 and T_2 , where $T_2 \geq T_1$ corresponds to the root $F_{16} = 0$, the free energy curve for $0 < \mu < \mu_{coin}$ (red and purple) includes two graphs that split $F_{16} = 0$. The two solutions are:-

$$\begin{aligned}
x_1 &= \frac{i\sqrt[3]{2}(\sqrt{3}+i)\left(\sqrt{81\mu^2R^2-12}-9\mu R\right)^{2/3}-2\sqrt[3]{3}(1+i\sqrt{3})}{2\ 6^{2/3}\sqrt[3]{\sqrt{81\mu^2R^2-12}-9\mu R}} \\
x_2 &= \frac{2i\sqrt[3]{3}(\sqrt{3}+i)-\sqrt[3]{2}(1+i\sqrt{3})\left(\sqrt{81\mu^2R^2-12}-9\mu R\right)^{2/3}}{2\ 6^{2/3}\sqrt[3]{\sqrt{81\mu^2R^2-12}-9\mu R}} \tag{3.55}
\end{aligned}$$

Putting x_1 and x_2 in the temperature T we get:-

$$T_1 = \frac{6\sqrt[3]{6}\left(\sqrt{81\mu^2R^2-12}-9\mu R\right)^{2/3}\left(\mu+\frac{\left(i\sqrt[3]{2}(\sqrt{3}+i)\left(\sqrt{81\mu^2R^2-12}-9\mu R\right)^{2/3}-2\sqrt[3]{3}(1+i\sqrt{3})\right)^3}{72R\left(\sqrt{81\mu^2R^2-12}-9\mu R\right)}\right)}{\pi\left(2\left(\sqrt[3]{3}+i3^{5/6}\right)-i\sqrt[3]{2}(\sqrt{3}+i)\left(\sqrt{81\mu^2R^2-12}-9\mu R\right)^{2/3}\right)^2} \tag{3.56}$$

$$T_2 = \frac{6\sqrt[3]{6}\left(\sqrt{81\mu^2R^2-12}-9\mu R\right)^{2/3}\left(\mu+\frac{\left(2i\sqrt[3]{3}(\sqrt{3}+i)-\sqrt[3]{2}(1+i\sqrt{3})\left(\sqrt{81\mu^2R^2-12}-9\mu R\right)^{2/3}\right)^3}{72R\left(\sqrt{81\mu^2R^2-12}-9\mu R\right)}\right)}{\pi\left(2i\sqrt[3]{3}(\sqrt{3}+i)-\sqrt[3]{2}(1+i\sqrt{3})\left(\sqrt{81\mu^2R^2-12}-9\mu R\right)^{2/3}\right)^2} \tag{3.57}$$

Putting μ equal to 0 we get $T_1 = \frac{1}{\pi R}$ and $T_2 = 0$. Furthermore, we see that the two temperatures are the same at the coincidence point where we don't obtain a graph. For this, $\mu_{coin} = \frac{1.5}{4R}$ so that we get the coincidence point as $T_{coin} = \frac{0.868}{\pi R}$. We have seen that when we put $\mu > \mu_{coin}$, we do not obtain any plots. So clearly plots are obtained when $\mu < \mu_{coin}$.

In Fig 13, the value of the x parameter raises along the graph up to the turning point at T_0 then decreases as we descend from the turning to the left coincidence point T_1 . As a result, the CFT state between the cusp and T_2 has a dip in entropy, but the state between the turning point and T_2 has an elevated entropy.

The entropy of the state between the turning point and T_1 is substantial. T_0 is the temperature at the stationary point, and it may be calculated as:-

$$\left(\frac{dT}{dx}\right)_\mu = 0 \quad \text{we get} \quad x_0 = \frac{\sqrt[3]{\mu}\sqrt[3]{R}}{\sqrt[3]{2}}$$

Hence we get the temperature at the cusp as $T_0 = \frac{3\sqrt[3]{\mu}}{2\sqrt[3]{2}\pi R^{2/3}}$

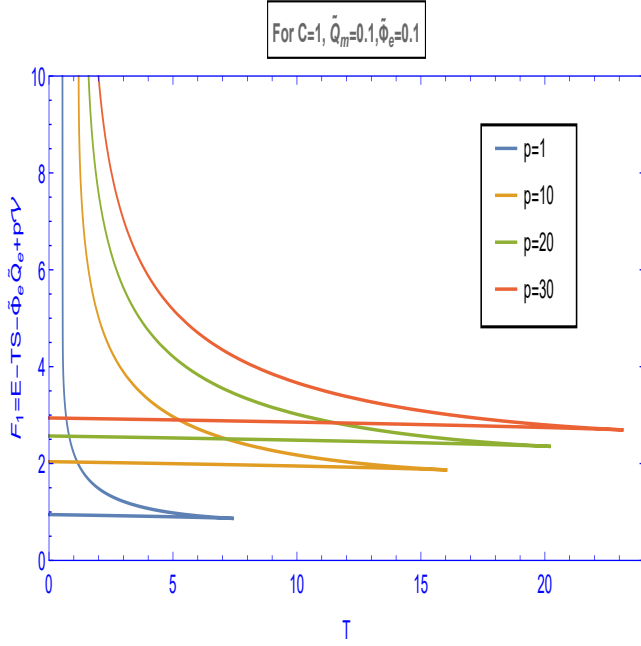
In this ensemble, there is just one change of phase for $\mu < 0$, but if we examine at $0 < \mu < \mu_{coin}$, we can see a change of phase that happens across both the branches having low and high entropy. Because as T_0 increases, the free energy of the higher entropy state diminishes. Then, the change of phase when the entropy goes from high to low occurs when the temperature of the CFT exceeds $T = T_1$, because beyond this temperature, only the branch having lower entropy remains, on the other hand, this transition is unusual because the entropy dips down during the process, which violates the law of thermodynamics, namely the second. When the temperature goes below $T = T_1$, the change of phase from the entropy branch of low- to high happens, and this change of phase appears more beneficial in the context of thermodynamics because we get an elevated entropy during the process.

4 The rest of the ensembles

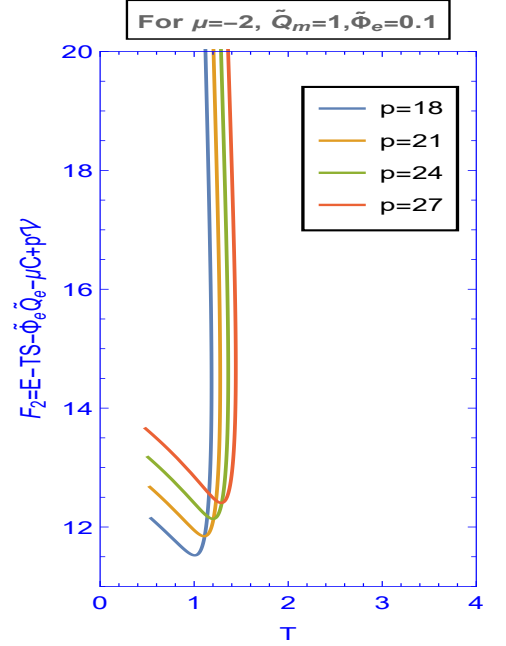
We have studied in earlier sections all the eight ensembles in detail. Also, there are eight more ensembles whose free energies are given in equation (3.1). Those free energies are namely $F_1, F_2, F_5, F_6, F_9, F_{10}, F_{13}, F_{14}$. In the figure given below, we have plot the graph of the free energy with respect to the temperature for all eight ensembles for different values of parameter. Now, if we put a certain condition like the infinite volume and temperature scenario where $TR \rightarrow \infty$, we can see many free energy equations change drastically, namely:-

$$F_1 = \tilde{\Phi}_m \tilde{Q}_m, \quad F_5 = \tilde{\Phi}_e \tilde{Q}_e, \quad F_9 = 0, \quad F_{13} = \tilde{\Phi}_e \tilde{Q}_e + \tilde{\Phi}_m \tilde{Q}_m \quad (4.1)$$

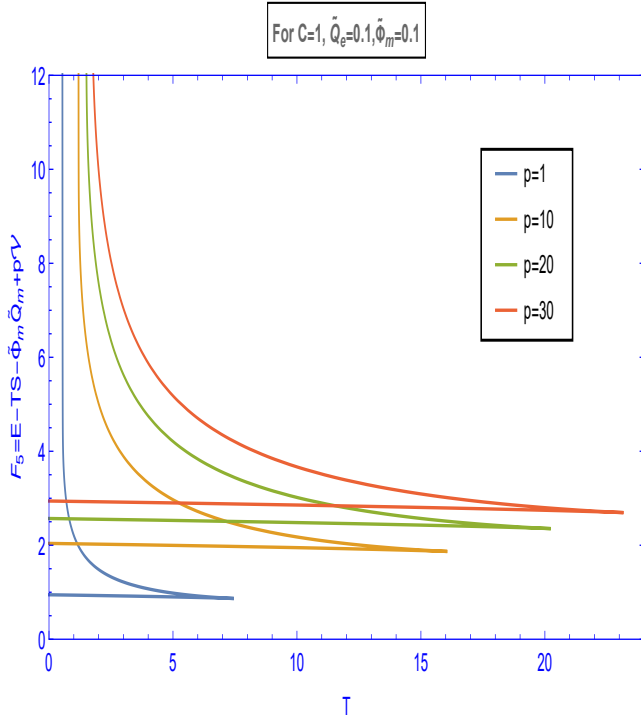
where $\mu C = -p\mathcal{V}$ in this boundary limit [62]. Also, we see that the free energy of F_1 corresponds to the free energy of F_4 in the $(\tilde{Q}_m, \tilde{\Phi}_e, \mathcal{V}, \mu)$ and F_5 corresponds to F_8 in the $(\tilde{\Phi}_m, \tilde{Q}_e, \mathcal{V}, \mu)$ and lastly F_{13} corresponds to the F_{16} in the $(\tilde{Q}_m, \tilde{Q}_e, \mathcal{V}, \mu)$ For the Fig (14) we examine the free energy plots against the temperature for various ensembles namely fixed $(\tilde{Q}_m, \tilde{\Phi}_e, p, C), (\tilde{Q}_m, \tilde{\Phi}_e, p, \mu), (\tilde{\Phi}_m, \tilde{Q}_e, p, C), (\tilde{\Phi}_m, \tilde{Q}_e, p, \mu)$ ensembles and for the figure (15), we plot for various ensembles for the fixed $(\tilde{\Phi}_m, \tilde{\Phi}_e, p, C), (\tilde{\Phi}_m, \tilde{\Phi}_e, p, \mu), (\tilde{Q}_m, \tilde{Q}_e, p, C), (\tilde{Q}_m, \tilde{Q}_e, p, \mu)$ ensembles. In fig (14) and (15), we notice that all the ensembles do not show phase transitions nor any critical phenomenon. Hence, we can say there is no critical behaviour in the ensembles of the CFT containing fixed p . Moreover, out of the eight ensembles, we notice that six ensembles namely at fixed $(\tilde{Q}_m, \tilde{\Phi}_e, p, C), (\tilde{Q}_m, \tilde{\Phi}_e, p, \mu), (\tilde{\Phi}_m, \tilde{Q}_e, p, C), (\tilde{\Phi}_m, \tilde{Q}_e, p, \mu), (\tilde{Q}_m, \tilde{Q}_e, p, C), (\tilde{Q}_m, \tilde{Q}_e, p, \mu)$ ensembles, therefore the free energy displays two separate branches. Here the down branch are analogous to a large black hole in the bulk which duals to a thermal state with high S/C , and the upper branch is analogous to the small AdS black hole which is dual to the thermal state with low S/C . The lower branch is more stable and this phase dominates because it has a low free energy value.



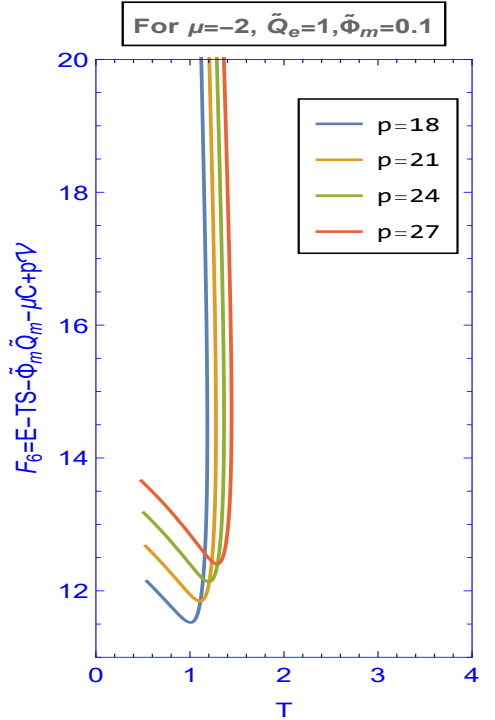
(a) F_1 vs \mathcal{T} plot for fixed $(\tilde{Q}_m, \tilde{\Phi}_e, p, C)$



(b) F_2 vs \mathcal{T} plot for fixed $(\tilde{Q}_m, \tilde{\Phi}_e, p, \mu)$

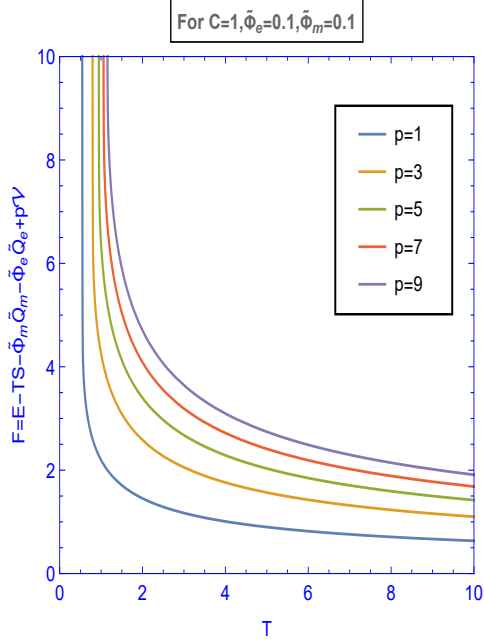


(c) F_5 vs \mathcal{T} plot for fixed $(\tilde{\Phi}_m, \tilde{Q}_e, p, C)$

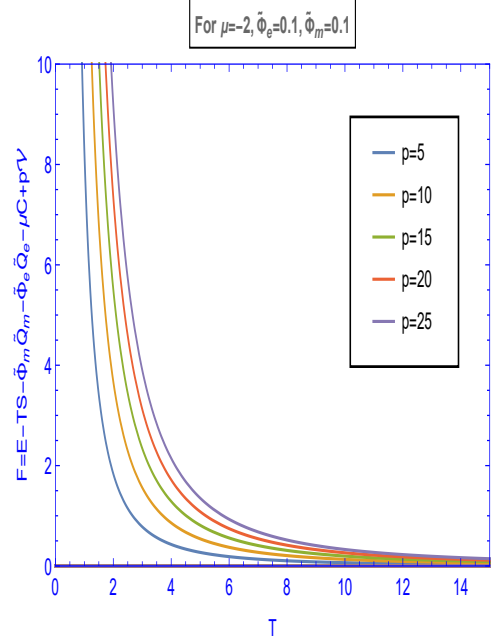


(d) F_6 vs \mathcal{T} plot for fixed $(\tilde{\Phi}_m, \tilde{Q}_e, p, \mu)$

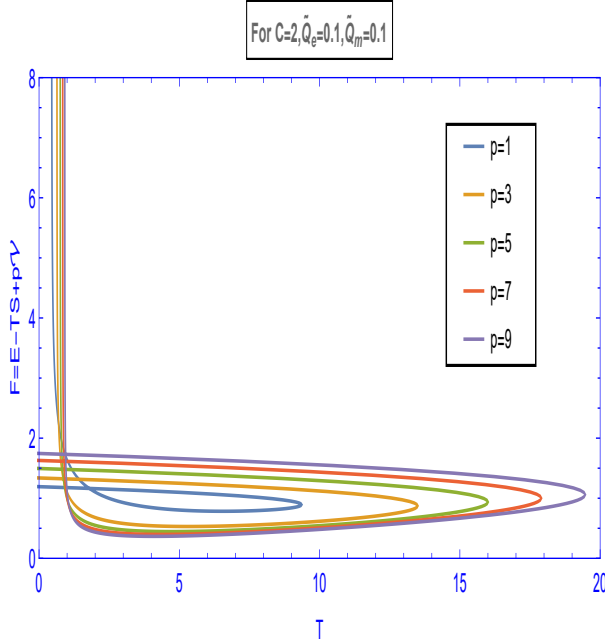
Figure 14: Free energy (F_1, F_2, F_5, F_6) vs \mathcal{T} plot for fixed $(\tilde{Q}_m, \tilde{\Phi}_e, p, C)$, $(\tilde{Q}_m, \tilde{\Phi}_e, p, \mu)$, $(\tilde{\Phi}_m, \tilde{Q}_e, p, C)$, $(\tilde{\Phi}_m, \tilde{Q}_e, p, \mu)$ ensembles



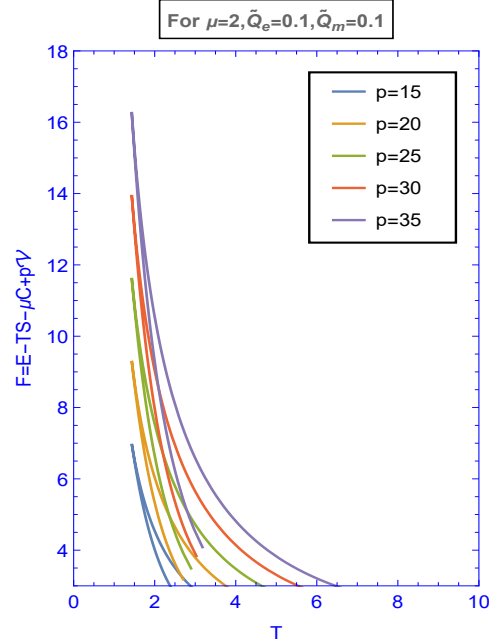
(a) F_9 vs \mathcal{T} plot for fixed $(\tilde{\Phi}_m, \tilde{\Phi}_e, p, C)$



(b) F_{10} vs \mathcal{T} plot for fixed $(\tilde{\Phi}_m, \tilde{\Phi}_e, p, \mu)$



(c) F_{13} vs \mathcal{T} plot for fixed $(\tilde{Q}_m, \tilde{Q}_e, p, C)$



(d) F_{14} vs \mathcal{T} plot for fixed $(\tilde{Q}_m, \tilde{Q}_e, p, \mu)$

Figure 15: Free energy ($F_9, F_{10}, F_{13}, F_{14}$) versus temperature \mathcal{T} plot for the fixed $(\tilde{\Phi}_m, \tilde{\Phi}_e, p, C)$, $(\tilde{\Phi}_m, \tilde{\Phi}_e, p, \mu)$, $(\tilde{Q}_m, \tilde{Q}_e, p, C)$, $(\tilde{Q}_m, \tilde{Q}_e, p, \mu)$ ensembles.

5 Discussions

We investigate the thermodynamics basically the change of phase of the CFT's in thermal states that are conjugate to charged Anti-de-Sitter black holes using the ADS/CFT correspondence. These conjugate thermodynamic variable pairs are connected to these thermal states: (T, S) , $(\tilde{\Phi}_e, \tilde{Q}_e)$, $(\tilde{\Phi}_m, \tilde{Q}_m)$, (p, \mathcal{V}) , and (μ, C) . According to the thermodynamic characteristics of the AdS black holes in the bulk, as seen via the holographic glossary, each of these combinations has a dual formulation. We studied each ensemble that was created and examined the parametric plots that were produced.

We only discovered critical behaviour in the ensembles $(\tilde{\Phi}_e, \tilde{Q}_m, \mathcal{V}, C)$, $(\tilde{\Phi}_e, \tilde{Q}_m, \mathcal{V}, \mu)$, $(\tilde{\Phi}_m, \tilde{Q}_e, \mathcal{V}, C)$, $(\tilde{\Phi}_m, \tilde{Q}_e, \mathcal{V}, \mu)$, $(\tilde{\Phi}_e, \tilde{\Phi}_m, \mathcal{V}, C)$, $(\tilde{Q}_m, \tilde{Q}_e, \mathcal{V}, C)$ and $(\tilde{Q}_m, \tilde{Q}_e, \mathcal{V}, \mu)$. Additionally, we get a zeroth-order phase transition between (small S/C) related to low entropy and (large S/C) related to high entropy phase has been seen in the ensembles $(\tilde{Q}_e, \tilde{Q}_m, \mathcal{V}, \mu)$, $(\tilde{\Phi}_e, \tilde{Q}_m, \mathcal{V}, \mu)$, $(\tilde{Q}_e, \tilde{\Phi}_m, \mathcal{V}, \mu)$ which we also observe in the paper [65].

For the fixed ensemble $(\tilde{Q}_m, \tilde{\Phi}_e, \mathcal{V}, C)$ we get a change of phase of the order of first and second. When we graph for various values of \tilde{Q}_m keeping rest parameters constant, we see a change of phase of order one for $\tilde{Q}_m < \tilde{Q}_m^{crit}$, a change of phase of second order for $(\tilde{Q}_m = \tilde{Q}_m^{crit})$ and nil phase transition for $(\tilde{Q}_m > \tilde{Q}_m^{crit})$. Similarly When we graph for numerous values of $\tilde{\Phi}_e$ while placing rest constrains constant, we see change of phase of order one for $\tilde{\Phi}_e < \tilde{\Phi}_e^{crit}$, a change of phase of order two for $(\tilde{\Phi}_e = \tilde{\Phi}_e^{crit})$ and nil phase transition for $(\tilde{\Phi}_e > \tilde{\Phi}_e^{crit})$. Finally, when we graph for numerous values of C keeping remaining constrains constant, we see a phase transition of the order of one for $C > C^{crit}$, a phase transition of the order of two for $(C = C^{crit})$ and nil phase transition for $(C < C^{crit})$

For the fixed ensemble $(\tilde{Q}_m, \tilde{\Phi}_e, \mathcal{V}, \mu)$, we graph for numerous values of μ while placing the rest constrains as constant. So when $\mu \leq 0$, we see only one phase, when $0 < \mu < \mu_{coin}$ we see a change of phase in between the two entropy branches for the low and high values. This high entropy branch ends at $T = T_1$ where after which we acquire a zeroth-order change of phase between the states of high and low entropy. This low entropy exists between $T_1 < T < T_2$.

For the fixed ensemble $(\tilde{Q}_e, \tilde{\Phi}_m, \mathcal{V}, C)$ we get a change of phase of the order of first and second. When we plot for various values of \tilde{Q}_m keeping rest parameters constant, we see a change of phase of first order for $\tilde{Q}_e < \tilde{Q}_e^{crit}$, a change of phase of second order for $(\tilde{Q}_e = \tilde{Q}_e^{crit})$ and nil phase transition for $(\tilde{Q}_e > \tilde{Q}_e^{crit})$. Similarly When we graph for numerous values of $\tilde{\Phi}_m$ placing rest constrains constant, we see a change of phase of order one for $\tilde{\Phi}_m < \tilde{\Phi}_m^{crit}$, a change of phase of second order for $(\tilde{\Phi}_m = \tilde{\Phi}_m^{crit})$ and nil phase transition for $(\tilde{\Phi}_m > \tilde{\Phi}_m^{crit})$. Finally, when we graph for numerous values of CFT's central charge C keeping rest parameters constant, we see change of phase of order one for $C > C^{crit}$, a change of phase of order two for $(C = C^{crit})$ and nil phase transition for $(C < C^{crit})$

For the fixed ensemble $(\tilde{Q}_e, \tilde{\Phi}_m, \mathcal{V}, \mu)$, we graph for numerous values of μ while maintaining the rest constrains as constant. So when $\mu \leq 0$, we see only one phase, when

$0 < \mu < \mu_{coin}$ we see a change of phase between two entropy branches having values both low and high. This high entropy branch ends at $T = T_1$ where after which we see a zeroth-order change of phase in the range of the entropy states having low and high values. This low entropy exists between $T_1 < T < T_2$.

For the fixed ensemble $(\tilde{\Phi}_e, \tilde{\Phi}_m, \mathcal{V}, C)$, we graph for numerous instances of $\tilde{\Phi}_e$ where we keep the rest as unchanged. We see a change of phase of the order one when the free energy changes sign at $F_{11} = 0$. There is a "confined" state when $F_{11} > 0$ and a "deconfined" state when $F_{11} < 0$. We get the same results when we plot the graph for diverge range of values of $\tilde{\Phi}_m$.

For the fixed ensemble $(\tilde{Q}_e, \tilde{Q}_m, \mathcal{V}, C)$ we get a change of phase of order one and two. When we plot for various values of \tilde{Q}_m keeping rest parameters constant, we see a change of phase of order one for $\tilde{Q}_e < \tilde{Q}_e^{crit}$, a change of phase of order two for $(\tilde{Q}_e = \tilde{Q}_e^{crit})$ and nil phase transition for $(\tilde{Q}_e > \tilde{Q}_e^{crit})$. Similarly When we graph for numerous range of values of \tilde{Q}_m keeping rest constrains static, we see a change of phase off order one for $\tilde{Q}_m < \tilde{Q}_m^{crit}$, a change of phase for order two for $(\tilde{Q}_m = \tilde{Q}_m^{crit})$ and nil phase transition for $(\tilde{Q}_m > \tilde{Q}_m^{crit})$. Finally, when we graph for a variety of values of C keeping rest variables constrains, we see change of phase of order one for $C > C^{crit}$, a change of phase of order two for $(C = C^{crit})$ and nil phase transition for $(C < C^{crit})$.

For the fixed ensemble $(\tilde{Q}_e, \tilde{Q}_m, \mathcal{V}, \mu)$, we graph for diverse range of values of μ while placing the rest constrains as static or constant. So when $\mu \leq 0$, we see only one phase, when $0 < \mu < \mu_{coin}$ we see change of phase between the entropy branches having low values and high values. This high entropy branch ends at $T = T_1$ where after which we see a zeroth-order phase transition between the high and low entropy states. This low entropy exists between $T_1 < T < T_2$.

We also plot the free energy plot for various ensembles namely $(\tilde{Q}_m, \tilde{\Phi}_e, p, C)$, $(\tilde{Q}_m, \tilde{\Phi}_e, p, \mu)$, $(\tilde{Q}_e, \tilde{\Phi}_m, p, C)$, $(\tilde{Q}_e, \tilde{\Phi}_m, p, \mu)$, $(\tilde{\Phi}_m, \tilde{\Phi}_e, p, C)$, $(\tilde{\Phi}_m, \tilde{\Phi}_e, p, \mu)$, $(\tilde{Q}_m, \tilde{Q}_e, p, C)$, $(\tilde{Q}_m, \tilde{Q}_e, p, \mu)$. Here we notice no phase transitions or any criticality which implies there is no $p - \mathcal{V}$ significance seen or criticality suggesting that the state of CFT which is conjugate to the dual charged Anti-de-Sitter black hole cannot be stated as a Van der Waals fluid.

In summary one can infer from this study that the study of the black hole thermodynamics is highly dependant on the choice of ensembles where we see different types of change of phase for different ensembles. Also for the CFT phase transitions for single charged black holes, we see 8 ensembles out of which we see phase transition in only 3. Whereas in this study we see 16 ensembles due to the introduction of magnetic charge making the study more rich and vibrant. Out of 16, we see phase transition in seven ensembles which is more due to the interactions of both the electric and magnetic charges which changes the thermodynamic potentials by introducing extra degrees of freedom. Due to this we get more ensembles and a larger and broader platform to study its rich phase structures

In future endeavours, we can check the interplay of the dyonic system with the addition of angular momentum and how the phase changes. We can also look this study from the

RPST formalism perspective. We can also look into the black holes of different models and study the CFT phase transitions.

References

- [1] J.D. Berkenstein, *Black holes and the second law*, *Lett. Nuovo. Cim.* **4** (1972) 737-740
- [2] J.D. Berkenstein, *Black holes and entropy*, *Phys. Rev. D* **7** (1973) 2333 [INSPIRE].
- [3] S.W. Hawking, *Particle creation by black holes*, *Commun. math. Phys.* **43** (1975) 199.
- [4] J. M. Bardeen, B. Carter, S. W. Hawking, *The four laws of black hole mechanics*, *Commun. Math. Phys.* **31** (1973) 161-170
- [5] S. W. Hawking, *Gravitational radiation from colliding black holes*, *Phys. Rev. Lett.* **26**, 1344-1346 (1971) doi:10.1103/PhysRevLett.26.1344
- [6] S. W. Hawking, *Black hole explosions*, *Nature* **248**, 30-31 (1974) doi:10.1038/248030a0
- [7] R. M. Wald, *Entropy and black-hole thermodynamics*, *Phys. Rev. D* **20**, 1271-1282 (1979) doi:10.1103/PhysRevD.20.1271
- [8] J. D. Bekenstein. *Black-hole thermodynamics*, *Physics Today*, **33**(1):24–31, 1980.
- [9] R. M. Wald, *The thermodynamics of black holes*, *Living Rev. Rel.* **4**, 6 (2001) doi:10.12942/lrr-2001-6 [arXiv:gr-qc/9912119 [gr-qc]]
- [10] S.Carlip, *Black Hole Thermodynamics*, *Int. J. Mod. Phys. D* **23**, 1430023 (2014) doi:10.1142/S0218271814300237 [arXiv:1410.1486 [gr-qc]]
- [11] A.C.Wall, *A Survey of Black Hole Thermodynamics*, [arXiv:1804.10610 [gr-qc]].
- [12] P.Candelas and D.W.Sciama, *Irreversible Thermodynamics of Black Holes*, *Phys. Rev. Lett.* **38**, 1372-1375 (1977) doi:10.1103
- [13] Chao Wang, Bin Wu, Zhen Ming Xu, Wen Li Yang, *Thermodynamic geometry of the RN-AdS black hole and non-local observables*, [arXiv:2210.08718]
- [14] Yuchen Huang, Jun Tao, Peng Wang, Shuxuan Ying, *Phase transitions and thermodynamic geometry of a Kerr-Newman black hole in a cavity*, *Eur.Phys.J.Plus* **138**, 265 (2023)[https://doi.org/10.1140/epjp/s13360-023-03858-w]
- [15] Wen-Xiang Chen, Yao-Guang Zheng, *Thermodynamic geometric analysis of BTZ black hole under $f(R)$ gravity*, [arXiv:2112.15032]
- [16] Peng Wang, Feiyu Yao, *Thermodynamic Geometry of Black Holes Enclosed by a Cavity in Extended Phase Space*, *Nucl. Phys. B*, **976** (2022) 115715 [https://doi.org/10.1016/j.nuclphysb.2022.115715]
- [17] Amin Dehyadegari, Ahmad Sheykhi, *Thermodynamic geometry and phase transition of spinning AdS black holes*, *Phys. Rev. D*, **104**, 104066, (2021) [doi:10.1103/PhysRevD.104.104066]
- [18] Shao-Wen Wei, Yu-Xiao Liu *General thermodynamic geometry approach for rotating Kerr anti-de Sitter black holes*, *Phys. Rev. D*, **104**, 084087 (2021) [10.1103/PhysRevD.104.084087]– 26
- [19] Seyed Ali Hosseini Mansoori, *Thermodynamic geometry of the novel 4-D Gauss Bonnet AdS Black Hole*, *Phys.Dark Univ.*, **31** (2021) 100776 [doi:10.1016/j.dark.2021.100776]

- [20] Aritra Ghosh, Chandrasekhar Bhamidipati, *Thermodynamic geometry for charged Gauss-Bonnet black holes in AdS spacetimes*, *Phys. Rev. D* **101**, 046005 (2020), [doi:10.1103/PhysRevD.101.046005]
- [21] Panah, B.E., Rodrigues, M.E. *Topological phantom AdS black holes in F(R) gravity*, *Eur. Phys. J. C* **83**, 237 (2023). <https://doi.org/10.1140/epjc/s10052-023-11402-4>
- [22] B. Eslam Panah, *Effects of energy dependent spacetime on geometrical thermodynamics and heat engine of black holes: gravity's rainbow* *Phys. Lett. B* **787** (2018) 45. [10.1016/j.physletb.2018.10.042]
- [23] Kh. Jafarzade, J. Sadeghi, B. Eslam Panah, and S. H. Hendi, "Geometrical thermodynamics and P-V criticality of charged accelerating AdS black holes" , *Annals of Physics* **432**, 168577 (2021).
- [24] Shao-Wen Wei and Yu-Xiao Liu. *Topology of black hole thermodynamics.*, *Phys. Rev. D* **105**:104003, (2022).
- [25] Shao-Wen Wei, Yu-Xiao Liu, and Robert B. Mann. *Black hole solutions as topological thermodynamic defects*, *Phys. Rev. Lett.*, **129**:191101,(2022).
- [26] B. Hazarika and P. Phukon, *Thermodynamic topology of black Holes in f(R) gravity*, *Progress of Theoretical and Experimental Physics*, **4**, (2024), <https://doi.org/10.1093/ptep/ptae035> [arXiv:2401.16756 [hep-th]].
- [27] N. J. Gogoi and P. Phukon, *Thermodynamic topology of 4D Euler-Heisenberg-AdS black hole in different ensembles*, [arXiv:2312.13577 [hep-th]]
- [28] B. Hazarika and P. Phukon, *Thermodynamic Topology of D = 4,5 Horava Lifshitz Black Hole in Two Ensembles*, [arXiv:2312.06324 [hep-th]].
- [29] B. Hazarika, N. J. Gogoi and P. Phukon, *Revisiting thermodynamic topology of Hawking-Page and Davies type phase transitions*, [arXiv:2404.02526 [hep-th]].
- [30] Di Wu, *Topological classes of rotating black holes*, *Phys. Rev. D* **107** (2023) 024024, arXiv: 2211.15151.
- [31] Di Wu, Shuang-Qing Wu, *Topological classes of thermodynamics of rotating AdS black holes*, *Phys. Rev. D* **107** (2023) 084002, arXiv: 2301.03002;
- [32] Di Wu, *Consistent thermodynamics and topological classes for the four-dimensional Lorentzian charged Taub-NUT spacetimes*, *Eur. Phys. J. C* **83** (2023) 589, arXiv: 2306.02324;
- [33] Di Wu, *Topological classes of thermodynamics of the four-dimensional static accelerating black holes*, *Phys. Rev. D* **108** (2023) 084041, arXiv: 2307.02030;
- [34] Di Wu, Shuang-Yong Gu, Xiao-Dan Zhu, Qing-Quan Jiang, Shu-Zheng Yang, *Topological classes of thermodynamics of the static multi-charge AdS black holes in gauged supergravities: Novel temperature-dependent thermodynamic topological phase transition*, *JHEP* **06** (2024) 213, arXiv: 2402.00106;
- [35] Behzad Eslam Panah, *Analytic Electrically Charged Black Holes in F(R)-ModMax Theory*, *Progress of Theoretical and Experimental Physics*, Volume 2024, Issue 2, February 2024, 023E01, <https://doi.org/10.1093/ptep/ptae012>
- [36] Bidyut Hazarika, B. Eslam Panah, Prabwal Phukon, *Thermodynamic topology of topological charged dilatonic black holes* [arXiv:2407.05325v1]

- [37] B.Eslam Panah, B.Hazarika, P.Phukon, *Thermodynamic topology of topological black hole in $F(R)$ -ModMax gravity's rainbow*, [<https://doi.org/10.48550/arXiv.2405.20022>]
- [38] J.M. Maldacena, *The large N limit of superconformal field theories and supergravity*, *Int. J. Theor. Phys.* **43** (1999) 1113 [*Adv. Theor. Math. Phys.* **43** (1998) 231] [[hep-th/971120](#)][INSPIRE].
- [39] S.W. Hawking and D. N. Page, *Thermodynamics of black holes in Anti-de Sitter space*, *Commun. Math. Phys.* **87** (1983) 577 [INSPIRE].
- [40] D. Kubiznak and R.B. Mann, *P - V criticality of charged AdS black holes*, *JHEP* **07** (2012)033 [[arXiv:1205.0559](#)] [INSPIRE].
- [41] B.P. Dolan, *Pressure and volume in the first law of black hole thermodynamics*, *Class. Quant. Grav.* **28** (2011) 235017 [[arXiv:1106.6260](#)] [INSPIRE].
- [42] B.P. Dolan, *The cosmological constant and the black hole equation of state*, *Class. Quant. Grav.* **28** (2011) 125020 [[arXiv:1008.5023](#)] [INSPIRE].
- [43] Dolan, *Compressibility of rotating black holes*, *Phys. Rev. D.* **84** (2011) 127503 [[arXiv:1109.0198](#)]
- [44] R.-G. Cai, L.-M. Cao, L. Li, R.-Q. Yang, *P - V criticality in the extended phase space of Gauss-Bonnet black holes in AdS space*, *JHEP* (2013) 005 [[arXiv:1306.6233](#)]
- [45] S. H. Hendi, S. Panahiyan, and B. Eslam Panah, *P - V criticality and geometrothermodynamics of black holes with Born-Infeld type nonlinear electrodynamics*, *Int. J. Mod. Phys. D* **25** (2016) 1650010. [[10.1142/S0218271816500103](#)]
- [46] S. H. Hendi, B. Eslam Panah, and S. Panahiyan, *Einstein-Born-Infeld-Massive Gravity: adS-Black Hole Solutions and their Thermodynamical properties*, *JHEP* **11** (2015) 157. ArXiv: [arXiv:1508.01311](#)
- [47] S. H. Hendi, R. B. Mann, S. Panahiyan, and B. Eslam Panah, *van der Waals like behaviour of topological AdS black holes in massive gravity*, *Phys. Rev. D* **95**, 021501(R) (2017). ArXiv: [arXiv:1702.00432](#)
- [48] D. Kubiznak, R.B. Mann and M. Teo, *Black hole chemistry: thermodynamics with Lambda*, *Class. Quant. Grav.* **34** (2017) 063001 [[arXiv:1608.06147](#)] [INSPIRE].
- [49] D. Kastor, S. Ray and J. Traschen, *Enthalpy and the mechanics of AdS black holes*, *Class. Quant. Grav.* **26** (2009) 195011 [[arXiv:0904.2765](#)] [INSPIRE].
- [50] E. Witten, *Anti-de Sitter space, thermal phase transition, and confinement in gauge theories*, *Adv. Theor. Math. Phys.* **2** (1998) 505 [[hep-th/9803131](#)] [INSPIRE].
- [51] A. Chamblin, R. Emparan, C. V. Jhonson and R. C. Myers, *Charged AdS black holes and catastrophic holography*, *Phys. Rev. D* **60** (1999) 064018 [[hep-th/9902170](#)] [INSPIRE].
- [52] A. Chamblin, R. Emparan, C. V. Jhonson and R. C. Myers, *Holography, thermodynamics and fluctuations of charged AdS black holes*, *Phys. Rev. D* **60** (1999) 104026 [[hep-th/9904197](#)] [INSPIRE].
- [53] M. Cvetič and S.S. Gubser, *Phases of R charged black holes, spinning branes and strongly coupled gauge theories*, *JHEP* **04** (1999)024 [[hep-th/9902195](#)] [INSPIRE].
- [54] B.P. Dolan, A. Kostouki, D. Kubiznak and R.B. Mann, *Isolated critical point from Lovelock gravity*, *Class. Quant. Grav.* **31** (2014)242001 [[arXiv:1407.4783](#)] [INSPIRE].

- [55] R.A. Hennigar, R.B. Mann and E. Tjoa, *Superfluid black holes*, *Phys. Rev. Lett.* **118** (2017) 021301 [arXiv:1402.2837] [INSPIRE].
- [56] N. Altamirano, D. Kubiznak, R.B. Mann and Z. Sherkatghanad, *Kerr-AdS analogue of triple point and solid/liquid/gas phase transition*, *Class. Quant. Grav.* **31** (2014)042001 [arXiv:1308.2672] [INSPIRE].
- [57] S.-W. Wei and Y.-X. Liu, *Triple points and phase diagrams in the extended phase of charged Gauss-Bonnet black holes in AdS space*, *Phys. Rev. D* **90** (2014)044057 [arXiv:1402.2837] [INSPIRE].
- [58] N Altamirano, D. Kubiznak and R.B. Mann, *Reentrant phase transition in rotating Anti-de Sitter black holes*, *Phys. Rev. D* **88** (2013)101502 [arXiv:1306.5756] [INSPIRE].
- [59] A.M. Frassino, D. Kubiznak, R.B. Mann and F. Simovic, *Multiple reentrant phase transitions and triple points in Lovelock thermodynamics*, *JHEP* **09** (2014)080 [arXiv:1406.7015] [INSPIRE].
- [60] C.V. Johnson, *Holographic heat engines*, *Class. Quant. Grav.* **31** (2014) 205002 [arXiv:1404.5982] [INSPIRE].
- [61] H. Xu, Y. Sun, L. Zhao, *Black hole thermodynamics and heat engines in conformal gravity*, *Int. J. Mod. Phys. D* **26** (2017) no.13, 1750151 [arXiv:1706.06442]
- [62] M.R. Visser, *Holographic thermodynamics requires a chemical potential for color*, *Phys. Rev. D* **105** (2022) 106014 [arXiv:2101.04145] [INSPIRE].
- [63] W. Cong, D. Kubiznak and R.B. Mann, *Thermodynamics of AdS Black Holes: Central Charge Criticality*, *Phys. Rev. Lett.* **127** (2021) 091301 [arXiv:2105.02223] [INSPIRE]
- [64] R. B. Alfaia, I. P. Lobo, L. C. T. Brito, *Central charge criticality of charged AdS black hole surrounded by different fluids*, *Eur. Phys. J. Plus* **137** (2022) 402 [arXiv:2109.06599] [hep-th]
- [65] W. Cong, D. Kubiznak, R.B. Mann and M.R. Visser, *Holographic CFT phase transitions and critically for charged AdS black holes*, *JHEP* **08** (2022) 174 [arXiv:2112.14848].
- [66] Gong, TF., Jiang, J., Zhang, M. *Holographic thermodynamics of rotating black holes*, *J. High Energy Phys.* 2023, 105 (2023). [https://doi.org/10.1007/JHEP06\(2023\)105](https://doi.org/10.1007/JHEP06(2023)105)
- [67] Moaathe Belhaj Ahmed, Wan Cong, David Kubiznak, Robert B. Mann, Manus R. Visser, *Holographic CFT Phase Transitions and Criticality for Rotating AdS Black Holes* [<https://doi.org/10.48550/arXiv.2305.03161>]
- [68] D. Kastor, S. Ray and J. Traschen, *Smarr formula and an extended first law for Lovelock gravity*, *Class. Quant. Grav.* **27** (2010) 235014 [arXiv:1005.5053] [INSPIRE].
- [69] D. Kastor, S. Ray and J. Traschen, , *Chemical potential in the first law for holographic entanglement entropy*, *JHEP* **11** (2014) 120 [arXiv:1409.3521] [INSPIRE].
- [70] A. Karch and B. Robinson, *Holographic black hole chemistry*, *JHEP* **12** (2015) 073 [arXiv:1510.02472] [INSPIRE].
- [71] D. Sarkar and M. Visser, *The first law of differential entropy and holographic complexity*, *JHEP* **11** (2020) 004 [arXiv:2008.12673] [INSPIRE].
- [72] Z. Gao, L. Zhao, *Restricted phase space thermodynamics for AdS black holes via holography*, *Classical And Quantum Gravity.*, 39, 075019 (2022)
- [73] Gao, Z., Kong, X., Zhao, L. *Thermodynamics of Kerr-AdS black holes in the restricted phase space*, *Eur. Phys. J. C* 82, 112 (2022). <https://doi.org/10.1140/epjc/s10052-022-10080-y>

- [74] Jafar Sadeghi, Mehdi Shokri, Saeed Noori Gashti, Mohammad Reza Alipour, *RPS Thermodynamics of Taub-NUT AdS Black Holes in the Presence of Central Charge and the Weak Gravity Conjecture*, [<https://doi.org/10.48550/arXiv.2205.03648>]
- [75] Md Sabir Ali, Sushant G. Ghosh, Anzhong Wang, *Thermodynamics of Kerr-Sen-AdS black holes in the restricted phase space* [<https://doi.org/10.48550/arXiv.2308.00489>]
- [76] Mozib Bin Awal, Prabwal Phukon, *Restricted Phase Space Thermodynamics of NED-AdS Black Holes*, [<https://doi.org/10.48550/arXiv.2404.03261>]
- [77] Y. Ladghami, B. Asfour, A. Bouali, A. Errahmani, T. Ouali, *4D-EGB black holes in RPS thermodynamics*, *Physics of the Dark Universe*, **41**, 2023, 101261, <https://doi.org/10.1016/j.dark.2023.101261>.
- [78] S. Dutta, A. Jain and R. Soni, *Dyonic black hole and holography*, *JHEP* **60** (2013) 07 [[arXiv:1310.1748](https://arxiv.org/abs/1310.1748)]
- [79] S. A. Hartnoll, C. P. Herzog and G. T. Horowitz, *Building an AdS/CFT superconductor*, *Phys. Rev. Lett.* **101** (2008) 031601 [[arXiv:0803.3295](https://arxiv.org/abs/0803.3295)] [[hep-th](#)]
S. A. Hartnoll, C. P. Herzog and G. T. Horowitz, *Holographic Superconductors*, *JHEP* **0812** (2008) 015 [[arXiv:0810.1563](https://arxiv.org/abs/0810.1563)] [[hep-th](#)]
- [80] S. A. Hartnoll, P. Kovtun, *Hall conductivity from dyonic black holes*, *Phys. Rev. D.* **76** (2007) 066001 [[arXiv:0704.1160](https://arxiv.org/abs/0704.1160)] [[hep-th](#)]
- [81] M. M. Caldarelli, O. J. C. Dias and D. Klemm, *Dyonic AdS black holes from magnetohydrodynamics*, *JHEP* **0903** (2009) 025 [[arXiv:0812.0801](https://arxiv.org/abs/0812.0801)] [[hep-th](#)]
- [82] Jeong, HS., Kim, KY., Sun, YW. *Quasi-normal modes of dyonic black holes and magneto-hydrodynamics*, *J. High Energ. Phys.*, **65** (2022). [https://doi.org/10.1007/JHEP07\(2022\)065](https://doi.org/10.1007/JHEP07(2022)065)
- [83] Ahn, Y.j., Baggioli, M., Huh, KB. et al. *Holography and magnetohydrodynamics with dynamical gauge fields*, *J. High Energ. Phys.*, **12** (2023). [https://doi.org/10.1007/JHEP02\(2023\)012](https://doi.org/10.1007/JHEP02(2023)012)
- [84] S. A. Hartnoll, P. K. Kovtun, M. Muller, S. Sachdev, *Theory of the Nernst effect near quantum phase transitions in condensed matter, and in dyonic black holes*, *Phys. Rev. B.* **76** (2007) 144502 [[arXiv:0706.3215](https://arxiv.org/abs/0706.3215)] [[cond-mat.str-el](#)]
- [85] M. Cvetič, G.W. Gibbons, D. Kubiznak and C.N. Pope, *Black hole enthalpy and an entropy inequality for the thermodynamic volume*, *Phys. Rev. D* **84** (2011) 024037 [[arXiv:1012.2888](https://arxiv.org/abs/1012.2888)] [[INSPIRE](#)].
- [86] D. Kubiznak and R.B. Mann, *Black hole chemistry*, *Can. J. Phys.* **93** (2015) 999 [[arXiv:1404.2126](https://arxiv.org/abs/1404.2126)] [[INSPIRE](#)].
- [87] J.-L. Zhang, R.-G. Cai and H. Yu, *Phase transition and thermodynamical geometry for Schwarzschild AdS black hole in $AdS^5 \times S_5$ spacetime*, *JHEP* **02** (2015) 143 [[arXiv:1409.5305](https://arxiv.org/abs/1409.5305)] [[INSPIRE](#)].
- [88] J.-L. Zhang, R.-G. Cai and H. Yu, *Phase transition and thermodynamical geometry of Reissner-Nordström-AdS black holes in extended phase space*, *Phys. Rev. D* **91** (2015) 044028 [[arXiv:1502.01428](https://arxiv.org/abs/1502.01428)] [[INSPIRE](#)].
- [89] B.P. Dolan, *Pressure and compressibility of conformal field theories from the AdS/CFT correspondence*, *Entropy* **18** (2016) 169 [[arXiv:1603.06279](https://arxiv.org/abs/1603.06279)] [[INSPIRE](#)].

- [90] B.P. Dolan, *Bose condensation and branes*, *JHEP* **10** (2014) 179 [arXiv:1406.7267] [INSPIRE].
- [91] J.P. Gauntlett, R.C. Myers and P.K. Townsend, *Black holes of $D = 5$ supergravity*, *Class. Quant. Grav.* **16** (1999) 1 [hep-th/9810204] [INSPIRE].
- [92] M.M. Caldarelli, G. Cognola and D. Klemm, *Thermodynamics of Kerr-Newman-AdS black holes and conformal field theories*, *Class. Quant. Grav.* **17** (2000) 3999 [hep-th/9908022] [INSPIRE].
- [93] E. Caceres, P.H. Nguyen and J.F. Pedraza, *Holographic entanglement chemistry*, *Phys. Rev. D* **95** (2017) 106015 [arXiv:1605.00595] [INSPIRE].
- [94] F. Rosso and A. Svesko, *Novel aspects of the extended first law of entanglement*, *JHEP* **08** (2020) 008 [arXiv:2003.10462] [INSPIRE].
- [95] M. Sinamuli and R.B. Mann, *Higher order corrections to holographic black hole chemistry*, *Phys. Rev. D* **96** (2017) 086008 [arXiv:1706.04259] [INSPIRE].
- [96] S.S. Gubser, I.R. Klebanov and A.M. Polyakov, *Gauge theory correlators from noncritical string theory*, *Phys. Lett. B* **428** (1998) 105 [hep-th/9802109] [INSPIRE].
- [97] E. Witten, *Anti-de Sitter space and holography*, *Adv. Theor. Math. Phys.* **2** (1998) 253 [hep-th/9802150] [INSPIRE].
- [98] I. Savonije and E.P. Verlinde, *CFT and entropy on the brane*, *Phys. Lett. B* **507** (2001) 305 [hep-th/0102042] [INSPIRE].
- [99] M. Henningson and K. Skenderis, *The holographic Weyl anomaly*, *JHEP* **07** (1998) 023 [hep-th/9806087] [INSPIRE].
- [100] V. Balasubramanian and P. Kraus, *A Stress tensor for Anti-de Sitter gravity*, *Commun. Math. Phys.* **208** (1999) 413 [hep-th/9902121] [INSPIRE].
- [101] V. P. Maslov, *Zeroth-order phase transitions*, *Math. Notes* **76** (2004) 697.